National Library of Canada
Acquisitions and Bibliographic Services Branch
395 Wellington Street
Ottawa, Ontario
K1A 0N4

Bibliothèque nationale du Canada
Direction des acquisitions et des services bibliographiques
395, rue Wellington
Ottawa (Ontario)
K1A 0N4

Your file Votre référence

Our file Notre référence

NOTICE

The quality of this microform is heavily dependent upon the quality of the original thesis submitted for microfilming. Every effort has been made to ensure the highest quality of reproduction possible.

If pages are missing, contact the university which granted the degree.

Some pages may have indistinct print especially if the original pages were typed with a poor typewriter ribbon or if the university sent us an inferior photocopy.

AVIS

La qualité de cette microforme dépend grandement de la qualité de la thèse soumise au microfilmage. Nous avons tout fait pour assurer une qualité supérieure de reproduction.

S'il manque des pages, veuillez communiquer avec l'université qui a conféré le grade.

La qualité d'impression de certaines pages peut laisser à désirer, surtout si les pages originales ont été dactylographiées à l'aide d'un ruban usé ou si l'université nous a fait parvenir une photocopie de qualité inférieure.

Canada

ISBN 0-612-04930-2

Canada

UNIVERSITÉ D'OTTAWA
UNIVERSITY OF OTTAWA

This thesis is dedicated to

my husband, Unni

and

my parents.

ACKNOWLEDGEMENTS

I wish to express my most sincere gratitude to my research supervisor, Dr. C. Paul Wilde, for his help and invaluable guidance throughout the course of this work. Many fruitful discussions with Dr. Wilde and his assistance during the preparation of this thesis are greatly acknowledged.

My sincere thanks are due to Mr. E. Kristoff and Mr. J. Hopkins for making the glass cells used in this work, Mr. F. Allard for building the electronic circuits, D. Hopkins for his help with mechanics and all members of the chemistry office for their administrative help.

I would like to thank my colleagues in this laboratory, M. Zhang, S. V. De Cliff, H. Al-Maznai and D. Yang for their help and support and for making the past three years I worked here memorable and enjoyable.

Above all, a very special thanks goes to my husband, Unni, and my parents for their love, patience and encouragement all the time.

CONTENTS

LIST OF FIGURES

ABSTRACT

This thesis describes the application of the Electrochemical Quartz Crystal Microbalance (EQCM) technique to the study of the electrochemistry of 4,4'bipyridyl at silver electrodes. The Ag-Bpy system was originally studied because Bpy was found to act as a promoter for the redox protein cytochrome c when adsorbed at silver electrodes. The system is also reported to display many phenomena (such as complex and film formation) that should be observable with the EQCM. The work presented here falls into two parts; the oxidation of silver in the presence of 4,4'bipyridyl and also the reduction of 4,4'bipyridyl at Ag electrodes.

Chapter 3 describes a study of the oxidation of Ag in the presence of 4,4'bipyridyl where the Ag^+ and bipyridyl form a complex. The application of cyclic voltammetry along with the EQCM which allows the measurement of mass changes (in the nanogram range) at electrode surfaces provide an interesting picture of the dissolution of Ag^+ and its subsequent complexation with 4,4'bipyridyl to form an Ag(I)-Bpy complex at the electrode surface. The observed mass changes are found to result from the superposition of a mass loss due to the release of Ag^+ into solution and a mass gain from complex precipitation. If the conditions of the experiment such as the scan

rate, upper potential limit and bipyridyl concentration are altered, the delicate balance between the above two processes switches and so dependent on conditions either a net mass loss or a net mass gain can be seen. At slower scan rates when the bulk bipyridyl concentration is 0.25mM, the balance between the processes switches twice in a narrow potential range causing the mass to decrease, increase, decrease and then increase again. These changes are mainly due to the slow accumulation of Ag^+ in the diffusion layer since not all the Ag^+ that is released is complexed.

When higher concentrations of Bpy (2mM) are used, complex formation is the dominant process that contributes to the mass change and so a simple mass increase is seen until the potential is extended further positive such that the surface concentration of bipyridyl is depleted significantly. Electrode corrosion then becomes the principal process causing the observed mass change to be a net decrease.

In Chapter 4, the reduction of 4,4'bipyridyl was studied at electrodeposited Ag electrodes in 0.1M Na_2SO_4. Thus in contrast to the oxidation experiments where silver is the redox active species, it is the bipyridyl that is the redox active species in the reduction experiments. At high negative potentials a film of reduced Bpy develops on the electrode surface and its growth, development and removal can be observed and

controlled by monitoring the mass responses. Although the reduction process is relatively straightforward, the re-oxidation process is quite complex, as revealed from the cyclic voltammograms. Complete removal of reduced Bpy film is not generally accomplished at the end of a cycle, but the re-oxidation process could be completed at quite negative potentials provided sufficient time is allowed. Cyclic voltammetric removal of thin films gives rise to a broad oxidation current stretching from -0.9V to 0.0V. When thicker films are removed in a similar manner, a noisy and uneven peak is observed which coincides with an increase in mass removal from the electrode surface. The position of this peak is dependent on the scan rate and potential. Possible causes of this unusual behaviour processes are discussed. Both systems studied provide an illustration of the extra insight into surface processes at electrodes that the EQCM method provides, relative to cyclic voltammetry alone.

PUBLICATIONS

1. "An EQCM Study of Corrosion and Complexation at Electrode Surfaces. Oxidation of Silver in the presence of 4,4'bipyridyl", C. P. Wilde and D. Pisharodi, *J. Electroanal. Chem.*, in press.

2. "Reduction of 4,4'bipyridyl at Ag electrodes - EQCM studies of film formation and removal", C. P. Wilde and D. Pisharodi, *J. Electroanal. Chem.*, in press.

CHAPTER 1

BASIC PRINCIPLES OF THE ELECTROCHEMICAL QUARTZ CRYSTAL MICROBALANCE TECHNIQUE

This thesis is concerned with an Electrochemical Quartz Crystal Microbalance (EQCM) study of corrosion and complexation at the surface of electrodes with reference to the oxidation of silver in the presence of 4,4'bipyridyl. The reduction of 4,4'bipyridyl at silver electrodes has also been studied and the formation of films of reduced bipyridyl on the electrode surface and their subsequent removal by oxidation are investigated. Since the Electrochemical Quartz Crystal Microbalance is the main technique used in this work, the basic principles of this technique will be presented in this chapter. A discussion of experimental methods is then presented in chapter 2 and the results are discussed in chapters 3 and 4.

1.1 Introduction.

In the past few years many new methods such as IR spectroscopy, X-Ray methods and the STM etc. have been applied to the study of

electrochemical interfaces[1]. The development of these methodologies has been stimulated by the significance of electrochemical interfacial processes in research and commercial applications (such as sensors, electroplating, corrosion, power sources etc.). The electrochemical quartz crystal microbalance (EQCM) is one of these methods which allows the in situ detection and monitoring of interfacial phenomena at the microscopic level. This is achieved through the sensitive measurement of mass changes as small as a few nanograms[2-6]. The electrochemical quartz crystal microbalance (EQCM) is an extension of the quartz crystal microbalance (QCM). The acronym EQCM is used for electrochemical measurements whereas the acronym QCM is used for non-electrochemical applications of the QCM technology. The QCM consists of a thin quartz crystal which is sandwiched between two metal electrodes (as shown in Figure 1) which allow the establishment of an alternating electric field across the crystal and its electrodes. The EQCM is identical, except for the fact that one of the two electrodes is also used as the working electrode in an electrochemical cell.

The quartz crystal microbalance is essentially a mass sensor and as such is a powerful technique that finds a wide variety of applications in different areas of technology[7]. For example, the QCM has been used in the detection of air pollutants (sulphur dioxide, hydrogen sulphide, hydrogen

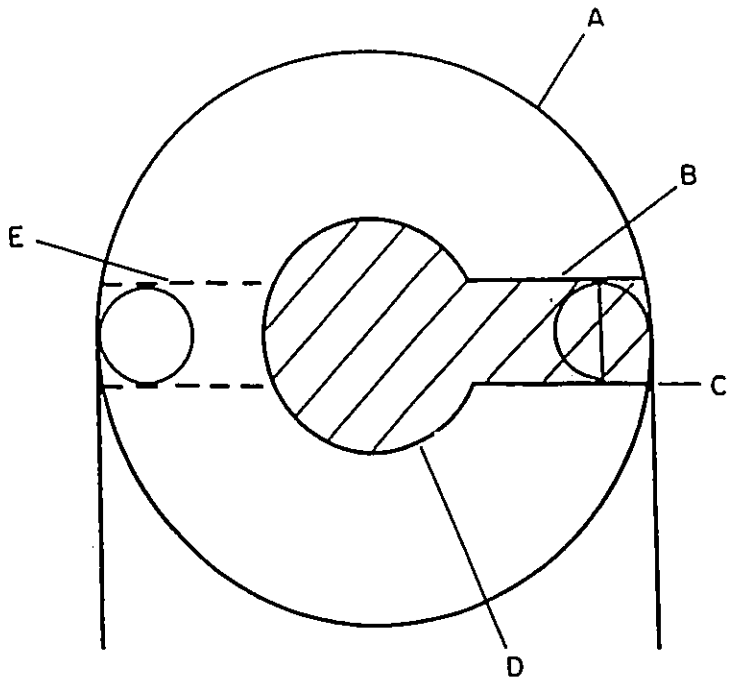

Figure 1. Piezoelectric quartz crystal with vacuum-deposited electrodes[4].

Gold is deposited on both sides of the quartz wafer (A) in the pattern shown. Electrical connection is made to the electrode flag (B) by means of a spring clip with attached lead (C). The circular gold electrode in the crystal centre (D) opposes an identical electrode on the other side of the crystal. Electrical connection to the opposing electrode is made to the electrode flag (E).

chloride, carbon monoxide, mercury, aromatic hydrocarbons, pesticides etc.)[8]. This is achieved by coating the quartz crystal with a substrate that will react with or adsorb the material of interest[9-11]. The QCM has also been used as a detector for chromatography due to its mass sensitivity and simplicity[12]. In addition, the QCM has been employed for the measurement of in situ metal electrodeposition and also provides a more convenient means for investigating fundamental processes such as the underpotential deposition (UPD) of metals[13]. The dissolution of metal films can be examined by the QCM hence its use as a corrosion sensor[14]. Finally, the QCM has been applied to the study of self-assembled monolayers, polymer films, dissolution and oxidation of metals[14-16], and enzymatic studies[17,18] etc., to name a few.

In this chapter we will describe the physical principles behind mass sensing for the QCM in the gas phase and then extend this model to discuss the effects of a contacting liquid on the operation of the QCM. This last aspect is important since in this thesis the QCM is operated in various electrolytes.

1.2 Use of the QCM as a mass sensor.

In the introduction it was stated that the QCM is a mass sensor, this

section describes the physical basis of the mass sensing action.

1.2.1 The Piezoelectric Effect.

The phenomenon of piezoelectricity was first observed by Pierre and Jacques Curie in 1880[19]. They discovered that when certain crystals are compressed in a particular direction, an electrical potential is produced between the deformed surfaces and this potential is found to be proportional to the applied pressure. This is known as the piezoelectric effect. Piezoelectricity is observed only in crystals that do not possess a centre of symmetry[20]. The pressure applied to a dielectric material distorts the crystal lattice, a separation of the centres of gravity of oppositely charged species occurs and this causes a dipole moment in each molecule. The converse piezoelectric effect which was first predicted by Lippmann[21] was later verified by the Curies. Here, the application of an electric field across a piezoelectric crystal results in a mechanical strain which is proportional to the applied potential. It is the converse piezoelectric effect that is the basis of the QCM.

1.2.2 Quartz Crystal Resonator.

The quartz crystal resonator is a piezoelectric wafer cut from a natural or synthetic single crystal of quartz. As described earlier, the application of a voltage across these crystals produces a corresponding mechanical strain and this results in the deformation of the material. This is schematically represented in Figure 2. On the other hand, the application of an *alternating* potential across the quartz crystal will produce mechanical *oscillations* within the crystal lattice. At the natural resonant frequency of the crystal, stable oscillations occur and at that frequency the crystal presents a low impedance to the driving voltage. If the crystal is incorporated into the feedback loop of an oscillating circuit containing an amplifier, it becomes the frequency determining element of the circuit. This system is then called a quartz crystal oscillator and this arrangement has been used in the experiments reported here. In the QCM, the quartz crystal wafer is sandwiched between two electrodes, typically gold, which allow imposition of the electric field. One of the electrodes deposited on the quartz wafer which is in contact with an electrolyte is used both to provide the alternating electric field which oscillates the crystal and also as the working electrode. The other electrode is exposed to air and it completes the oscillation circuit. This arrangement allows the measurement of potential, current, charge and the frequency changes at the working electrode.

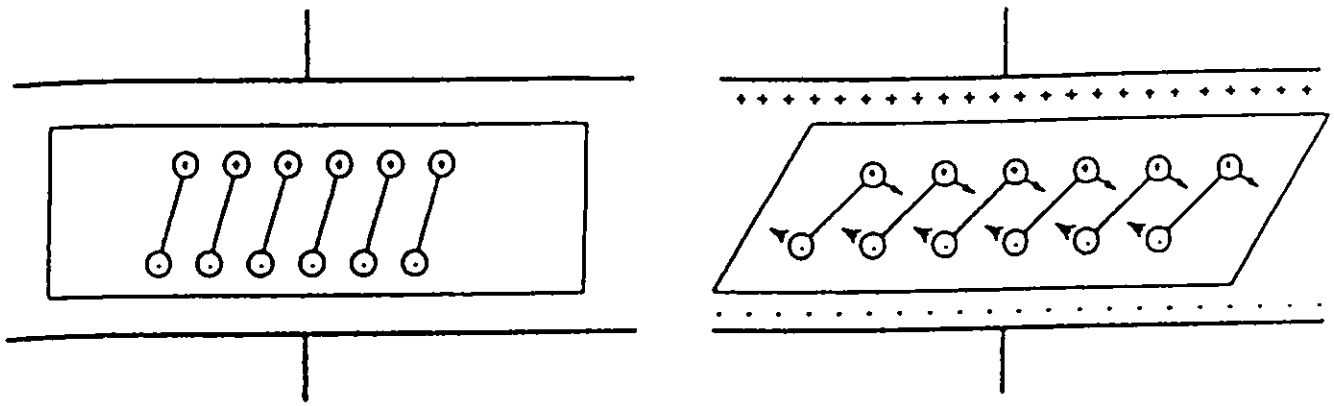

Figure 2. Schematic representation of the converse piezoelectric effect for shear motion[13].

1.2.3 The Thickness Shear Mode of Vibration.

A piezoelectric quartz crystal resonator can have many modes of resonance or standing wave patterns at the resonant frequencies. In the QCM, the most useful mode of vibration is the high frequency thickness-shear mode, as it is most sensitive to the addition or removal of mass. The thickness-shear vibration in the fundamental mode is illustrated in Figure 3. By careful design, quartz crystal resonators with all unwanted modes sufficiently suppressed and separated from the principal thickness-shear mode can be obtained. This can be achieved if the plate is cut to a specific orientation with respect to the crystal axes. The mode of resonance of the quartz crystal plate is not much altered by a small change in the orientation of the crystal with respect to the crystallographic axes, but the temperature and stress coefficients of the quartz crystal are critical functions of the angle of cut. The frequency of oscillation of the quartz crystal depends on the physical dimensions of the quartz crystal and the thickness of the electrodes deposited on it. For use as a QCM or EQCM, AT- or BT- cut quartz plates (AT and BT refer to the orientation of the quartz wafer with respect to the crystal axes), are found to be most useful[23] since these plates have low or

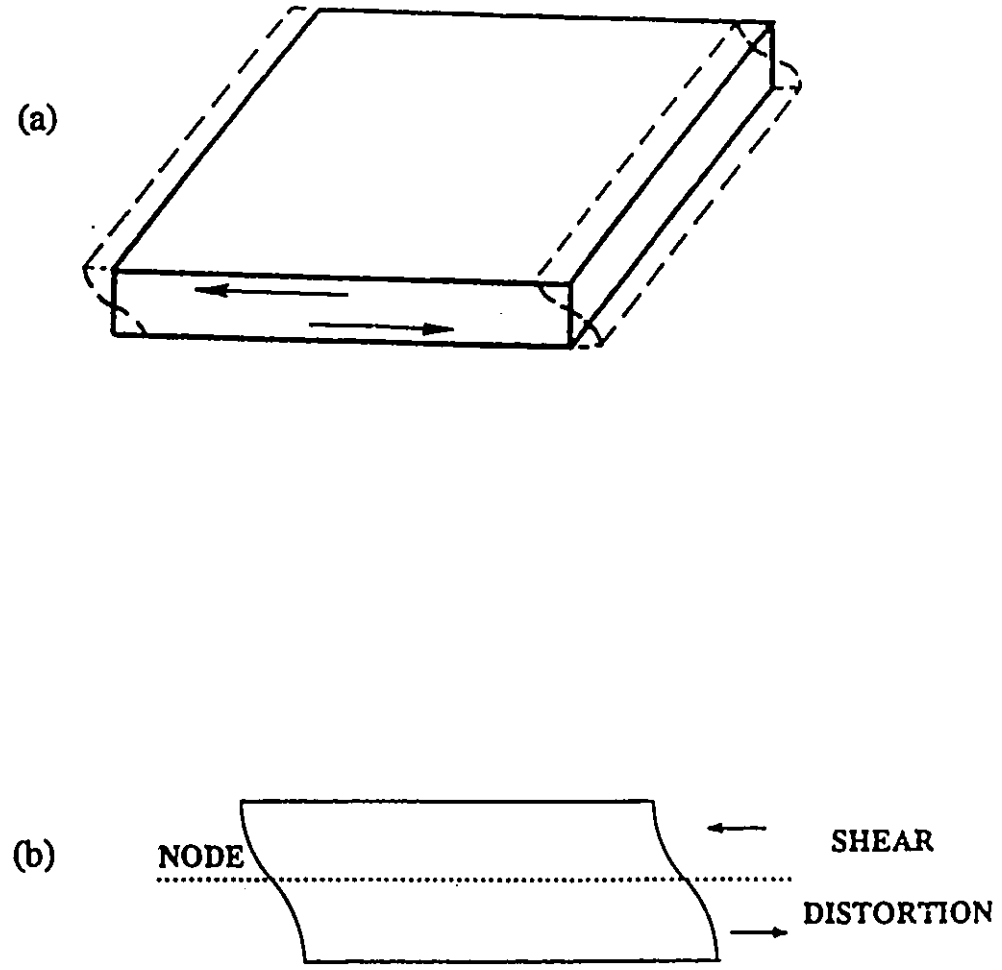

Figure 3. (a) The fundamental thickness-shear mode of vibration[7]. (b) Edge view of QCM disk showing shear deformation[22].

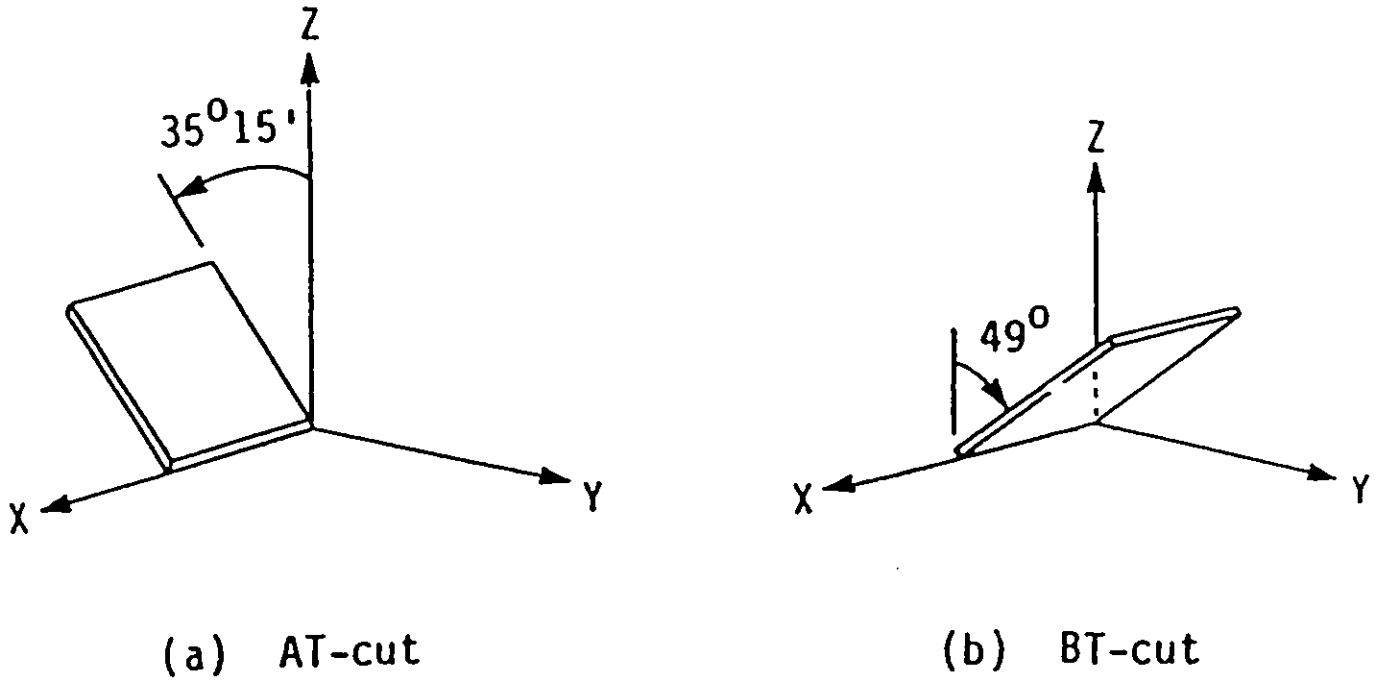

Figure 4. AT- and BT-cut quartz crystal plates[7].

zero temperature coefficients at room temperature. AT-cut (+35°15') and BT-cut (-49°00') wafers are shown in Figure 4. The AT-cut is superior to the BT-cut in temperature coefficient and mass sensitivity[24]. AT-cut crystals that oscillate in the thickness-shear mode are used in the work reported here.

1.2.4 Operation of the QCM in the gas phase.

For the successful operation of the QCM in the gas phase, a quantitative relationship between the mass and frequency must be known. An equation relating frequency and mass changes was first derived by Sauerbrey[25,26], based on the idealized physical model shown in Figure 5. When a quartz crystal plate oscillates in the fundamental thickness-shear mode, the thickness of the plate can be related to the resonant wavelength by the following equation,

$$t_q = \lambda_q/2 \qquad (1.1)$$

where t_q is the thickness of the plate and λ_q is the wavelength of the shear-mode elastic wave in the thickness direction. In terms of the resonant frequency f_q and the velocity of propagation of the shear wave v_q, the

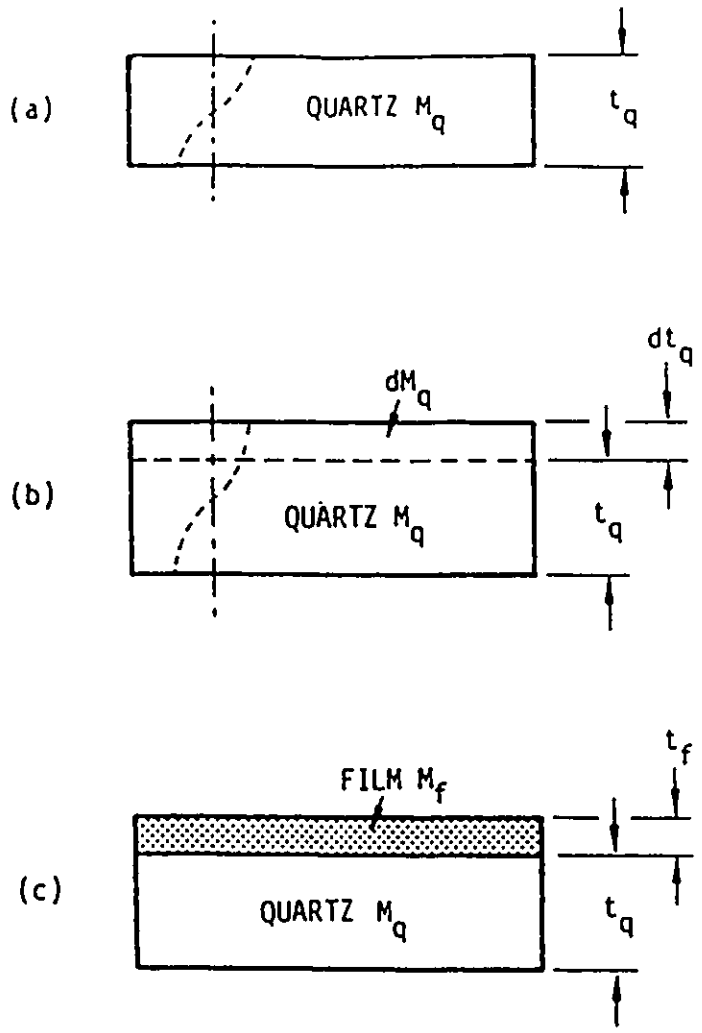

Figure 5. A simplified model of a quartz crystal microbalance[7].

(a) At resonance, the wavelength is equal to half of the quartz plate thickness. (b) An increase in the quartz plate thickness results in a decrease in the resonant frequency (an increase in the wavelength). (c) The mass of a deposited film is treated as an equivalent amount of the quartz mass.

equation (1.1) can be written as,

$$f_q\, t_q = v_q/2 \qquad (1.2)$$

since

$$\lambda_q\, f_q = v_q \qquad (1.3)$$

From equation (1.2), the shift in the resonant frequency df_q caused by an infinitesimal change in the crystal thickness dt_q is given by,

$$df_q/f_q = -dt_q/t_q \qquad (1.4)$$

The negative sign arises because (1.1) shows that the wavelength increases and so the resonant frequency of the quartz wafer decreases with increasing thickness of the plate.

$$t_q = M_q/\rho_q \qquad (1.5)$$

The density and mass of the crystal are related by the equation (1.5), where M_q is the mass of the quartz crystal per unit area and ρ_q is the density of the

quartz crystal (2.648 gcm^{-3}). Substituting a differential form of (1.5) into (1.4) gives,

$$df_q/f_q = -dM_q/M_q \qquad (1.6)$$

Sauerbrey made the assumption that a small mass change due to a foreign layer (dM rather than dM_q) can be treated as an equivalent mass change of the quartz crystal itself. Equation (1.6) thus becomes,

$$df_q/f_q = -dM/M_q \qquad (1.7)$$

where dM is an infinitesimal amount of foreign mass uniformly distributed over the crystal surface. If we define the areal densities m_f and m_q as the mass per unit area for the deposited layer and the quartz crystal respectively, (1.7) can be written as,

$$df_q/f_q = -m_f/m_q \qquad (1.8)$$

For materials with a density which is spatially uniform, (1.8) can be arranged to give

$$\Delta f = -2\ \Delta m\ f_q^2/\rho_q\ v_q\ A \qquad (1.9)$$

Since the shear wave velocity v_q and the shear modulus of quartz μ_q (2.947×10^{11} $gcm^{-1}s^{-2}$) are related by the equation,

$$v_q = (\mu_q/\rho_q)^{1/2} \qquad (1.10)$$

(1.9) can be written as,

$$\Delta f = -2\ \Delta m\ f_0^2/A\ (\mu_q\ v_q)^{1/2} \qquad (1.11)$$

where f_0 is the fundamental frequency of the crystal (f_0 is equivalent to f_q). Equation (1.11) is called the Sauerbrey equation. Substituting the values for the constants in equation (1.11) and letting $A = 1cm^2$ gives

$$\Delta f = -2.26 \times 10^{-6}\ f_0^2\ \Delta m \qquad (1.12)$$

From equation (1.12) the mass sensitivity calculated for a 10MHz quartz crystal wafer (used in this work) is 0.226 $Hzcm^2ng^{-1}$, i.e. 4.42 $ngHz^{-1}cm^{-2}$. The Sauerbrey equation thus relates the change in the resonant frequency of

the quartz crystal oscillator (Δf) to the change in mass (Δm) of the film on the crystal surface. The negative sign in (1.12) indicates that the frequency decreases as the mass increases.

Sauerbrey's theory has been experimentally verified for thin rigid overlayers attached to a QCM exposed to vacuum. In these cases, Δf changes linearly with Δm since the physical properties of the deposits such as mechanical stress and damping do not affect the material constants of quartz (μ_q and ρ_q) significantly. Sauerbrey's equation has been successfully applied for thin overlayers up to a mass load of 2% of the mass of the unloaded crystal. When the overlayers are thicker, the relation of Δf to Δm is non-linear and a more complicated theory is required[27].

1.2.5 Effect of contact with liquid.

The theory discussed above has been successfully employed in the application of the QCM in the gas phase. The successful operation of the QCM in liquids was initially considered to be unlikely because of the damping effects caused by the liquid which has a higher viscosity than any gas which contacts the electrode. However, in 1980, Konash and Bastiaans[28] and in 1981 Nomura[29], verified the operation of the QCM in a liquid

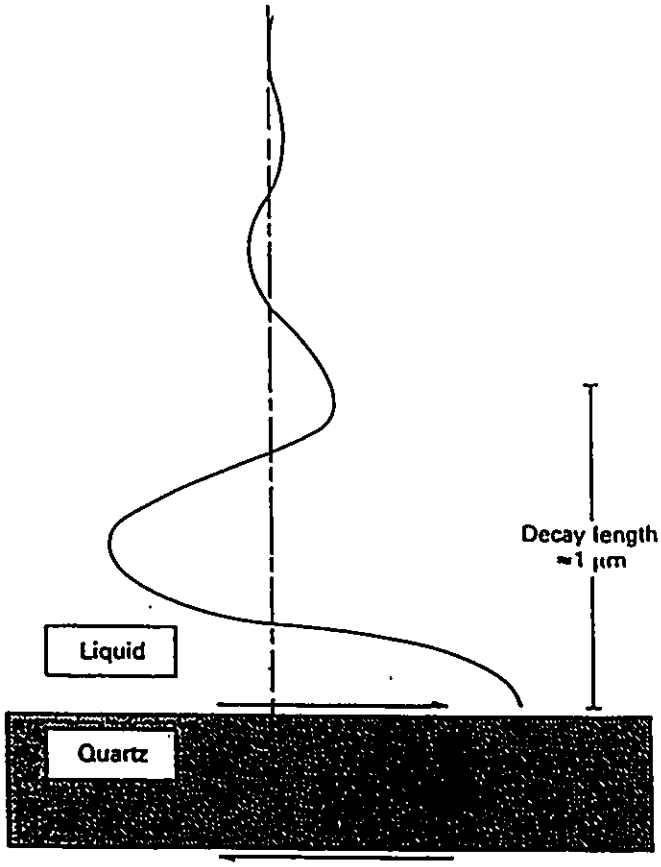

Figure 6. Propagation of the transverse shear wave from the QCM into a liquid[33].

environment. When one face of the quartz crystal resonator is in contact with a viscous liquid, a change in resonant frequency occurs that is predicted to be dependent on the density and viscosity of the liquid[30]. K.Kanazawa and J.Gordon[31,32] have analyzed how the viscous coupling effects between the QCM and the liquid affect the oscillations of the quartz crystal in terms of the density and viscosity of the liquid. In their simple physical model, the quartz crystal is treated as a lossless elastic solid and the liquid as a purely viscous medium. The resulting change in frequency upon immersion arises from the coupling of the standing shear wave of the oscillating crystal to the liquid. This results in a damped shear wave travelling normal to the crystal surface in the viscous medium, as shown in Figure 6. The atomic displacements corresponding to this shear motion are thus parallel to the crystal surface.

Under the assumption that the transverse velocity of the quartz surface is identical to that of the adjacent fluid layer (this is referred to as the "no slip" condition) and also that the shear wave in solution decays exponentially with a characteristic decay length (typically less than 1μm) the change in frequency Δf when one face of the quartz crystal is in contact with the liquid is given by,

$$\Delta f = -f_0^{3/2} [\eta_L \rho_L / \pi \mu_q \rho_q]^{1/2} \qquad (1.13)$$

where f_0 is the fundamental frequency of the crystal in air and η_L and ρ_L are the viscosity and density of the solution respectively. μ_q is the shear modulus of quartz and ρ_q its density. By substituting the numerical values of μ_q and ρ_q into equation (1.13) we find

$$\Delta f = -6.39 \times 10^{-7} f_0^{3/2} (\eta_L \rho_L)^{1/2} \qquad (1.14)$$

S.Bruckenstein and M.Shay[4] derived a similar relationship based on dimensional analysis, given by,

$$\Delta f = -2.26 \times 10^{-6} f_0^{3/2} (\eta_L \rho_L)^{1/2} \qquad (1.15)$$

A decrease of the oscillating frequency of the quartz crystal upon immersion in a viscous liquid is predicted by both treatments discussed above. Kanazawa and Gordon's theory predicted a frequency decrease of 2 kHz for a 10 MHz AT-cut quartz crystal in pure water at 20°C. On the other hand, Bruckenstein and Shay's model predicted a frequency decrease of 7 kHz. Simple experiments performed in our lab show a frequency decrease

of ~7 kHz for a 10 MHz quartz crystal when in contact with an electrolyte. The reasons for the discrepancy in the predicted values by the above treatments are still uncertain. However, both theories predict a frequency decrease of the quartz crystal upon immersion in a liquid. This frequency decrease is proportional to $(\rho_L \eta_L)^{1/2}$ as given in (1.14) and (1.15). By keeping the solution composition and temperature unaltered throughout the course of the experiments (so that neither ρ_L or η_L changes) the frequency offset resulting from the presence of solution should also remain constant and the Sauerbrey equation can still be used. Any added foreign mass is assumed to cause a change in the resonant frequency of the quartz crystal according to the Sauerbrey equation. This is the basis of the EQCM method used in the present work.

The discussion in the previous paragraph has shown that a constant frequency offset is produced by immersing the QCM in a liquid. Although the typical decay length of the shear wave in solution is about 1 micron it is possible that a column of liquid could exert stress on the crystal. However, Bruckenstein and Shay[4] investigated the effect of the height of the liquid above the quartz crystal on the frequency change. They measured the frequency change after each addition of successive amounts of water to the electrochemical cell to increase the total liquid column height up to 11.2 cm

and found that the effect was negligible. Thus the frequency of an AT-cut quartz crystal is insensitive to solution volume and the height of a column of liquid above the crystal.

1.2.6 Non-ideal behaviour of the QCM.

Apart from the density and viscosity effects of the liquid, there are other parameters which could cause frequency changes of the quartz crystal. Such non-ideal behaviour (meaning that the frequency change does not result from a mass change) of the QCM can be caused by several factors including viscoelastic properties, surface roughness and porosity, surface stress, interfacial slippage, high mass loading etc. as shown in Figure 7. Some of these properties will be discussed here very briefly.

Viscoelastic properties : Viscoelastic properties have been exhibited by electrodes coated with thick polymer films or adsorbed enzymes[13]. The unexpected increase in Δf values for such electrodes is attributed to changes in mechanical properties of the polymer film with a corresponding change in $\eta_f\mu_f$ (η_f is the viscosity and μ_f is the shear modulus of the film). Such viscoelastic interferences in EQCM experiments have not been extensively studied so far.

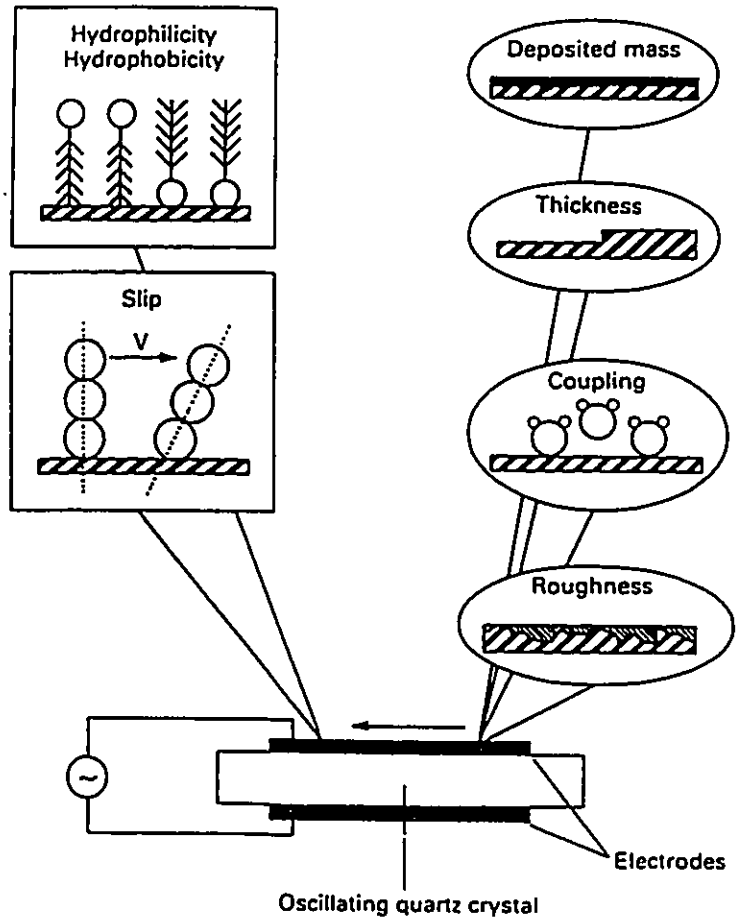

Figure 7. Schematic diagram of interfacial factors that govern the behaviour of the oscillating quartz crystal in the liquid phase[33].

Surface roughness and porosity : The surface roughness and porosity of QCM electrodes can influence the amount of liquid trapped in the surface cavities. Thus if surface roughness changes during an experiment, it can give rise to high mass loadings whose magnitude will depend upon the amount of liquid trapped and the size of the cavities. However, this effect is only significant *if* the surface roughness changes during an experiment. This aspect of the QCM is discussed further in chapter 3.

Interfacial slippage : The first layer of solvent at the QCM metal electrode surface is assumed to be tightly bound against the metal surface and so it does not slip during the shear motion of the crystal. This is referred to as the "no slip" condition. Thus, the vibrating QCM electrode and the adjacent molecular layer of the liquid move at the same velocity. The decay length of the shear wave and the effective thickness of the liquid layer will be affected in the case of any interfacial slippage. However, the frequency of the QCM has not been quantitatively related to the slippage effect, so far, and it is very difficult to detect an effect of slippage unless frequency changes are very different from expected values.

In such circumstances of non-ideal behaviour as discussed above, the frequency response of the QCM does not obey Sauerbrey equation. However, in most QCM investigations, it is assumed that ideal rigid layer behaviour

is observed at the electrode surface when interpreting frequency changes using the Sauerbrey equation. In all QCM experiments it is important to assess the QCM response to see if it is the response expected from a consideration of the chemistry or electrochemistry of the system. For example, if a metal is deposited on the QCM, the charge passed can be used with Faraday's Law to predict the expected mass gain. QCM responses that appear unusual after such a comparison are usually due to non-ideal behaviour of some type but most types of non-ideal behaviour are very hard to measure or study.

In the present work, the contributions from the non-ideal behaviour are made largely negligible by conducting the experiments at constant temperature and also by using a constant volume of liquid in the electrochemical cell.

CHAPTER 2

EXPERIMENTAL

2.1 Quartz Crystals.

10 MHz fundamental AT-cut crystals were used. The crystals were obtained from the International Crystal Manufacturing Company Inc., Oklahoma City. The crystals were finished with 5 micron abrasive and had about 900 Å of gold vacuum-deposited on each face, by the manufacturer.

2.2 Electrodes.

The working electrodes used in this study were silver electrodes plated onto the deposited gold electrode of the crystal. Prior to plating, these gold electrodes were cleaned in 0.1M $HClO_4$ by cycling between 0.0 and 1.4V at 50 mVs^{-1} until a stable cyclic voltammogram was obtained. The electrochemical cell was then thoroughly rinsed with Milli-Q water and the gold electrode was plated with silver. The galvanostatic plating was done using either a non-cyanide plating bath[34] or a 1mM solution of $AgNO_3$ in

0.1M $HClO_4$ by passing 50 μA for 400s. In some cases, the silver was plated potentiostatically by holding the potential such that about 50 μA reduction current was passed. The results obtained were generally not affected by the method of plating. The electrodes were then rinsed with Milli-Q water and then dried in a stream of nitrogen. The counter (auxiliary) electrode used was a silver wire although for the plating process Au wire was used. The reference electrode was a saturated calomel electrode (SCE) separated from the cell by a Luggin capillary. All potentials in this work are referred to the SCE.

2.3 Electrochemical cells and Instrumentation.

A diagram of the electrochemical cell is shown in Figure 8. It is a Pyrex glass cell with four openings at the top; two for the connections of the counter electrode and the Luggin capillary and the other two for the circulation of nitrogen gas in and out of the cell. The quartz crystal is mounted at the bottom of the cell using a silicone sealant, taking much care to avoid the contact of the sealant with the electrode surface. One face of the quartz crystal which is in contact with the solution serves as the working electrode and the other face is exposed to air. The quartz crystal is then

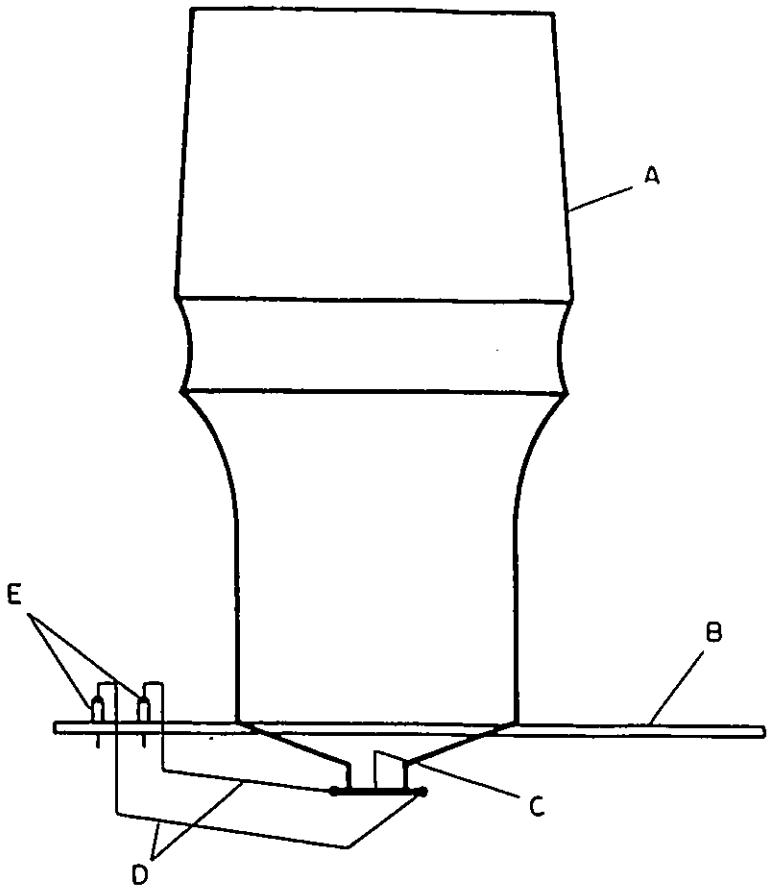

Figure 8. Lower half of the electrochemical cell with attached crystal[4].

(A) Ground glass joint for connection to Luggin capillary, counter electrode chamber and solution bubbler; (B) a plug-board cemented to the glass; (C) quartz crystal attached to the opening of the glass cell; (D) rigid leads connecting the crystal to plug-board jacks; (E) plug-jacks to connect the crystal to the oscillator circuit board.

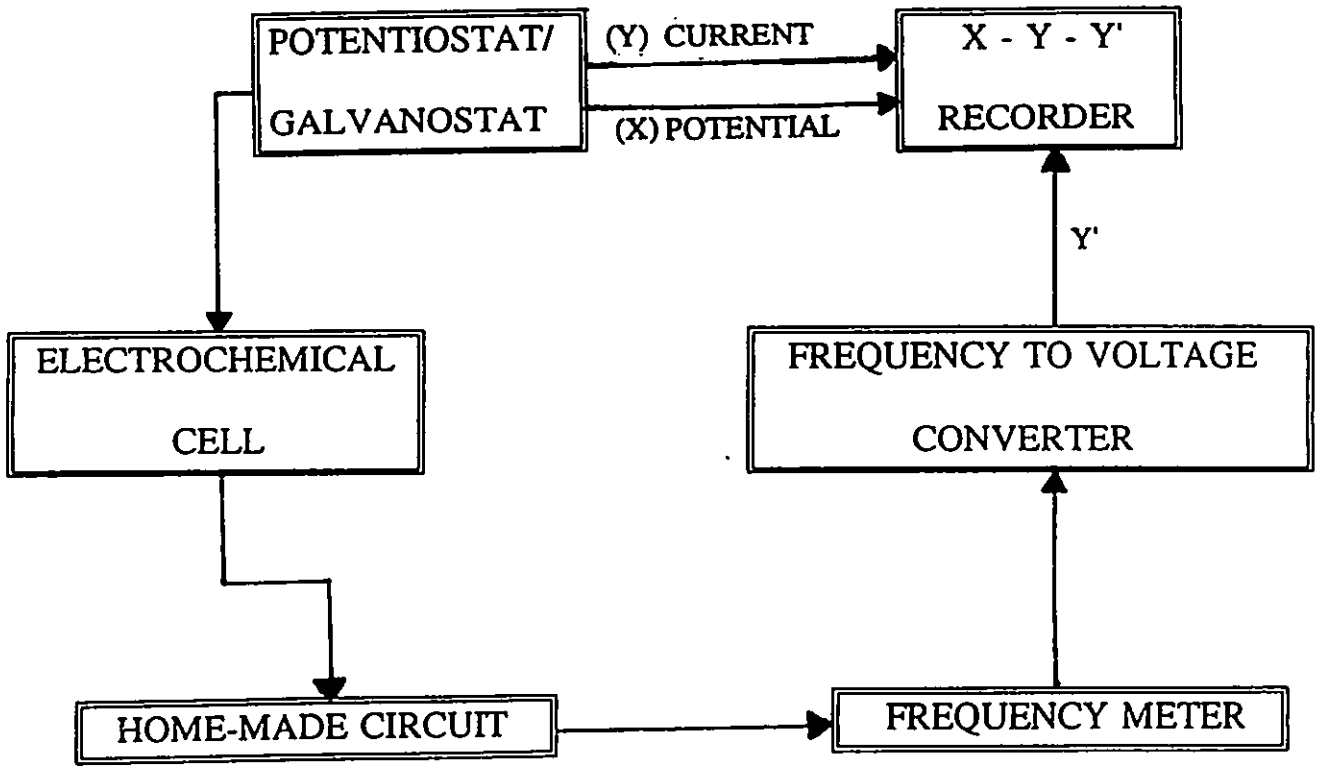

Figure 9. Schematic diagram of the EQCM apparatus.

connected to the oscillating circuit (similar to the one reported by Bruckenstein and Shay[4]) for the EQCM which is driven by a DC voltage supply of 5.0V.

The arrangement of the EQCM is shown in Figure 9. The frequency difference between the working crystal and the reference crystal is converted to a voltage by a home-built frequency-to-voltage converter[4]. This voltage signal is then displayed either on a Kipp and Zonen BD91 or a Philips PM 8272 X-Y-Y' recorder. The current and potential are also recorded simultaneously. An Oxford Electrodes bipotentiostat (Abington, England) was used for the potential control.

The frequency-to-voltage converter was calibrated by connecting it to a frequency generator and then measuring the corresponding voltage response. The voltage was then plotted as a function of frequency (as shown in Figure 10) and was found to be linear up to a frequency of 60 kHz. From the slope of the line, the frequency sensitivity was found to be 61.5 mV/kHz or 16.2 Hz/mV.

2.4 Calibration of the EQCM.

The calibration of the EQCM was performed by the galvanostatic

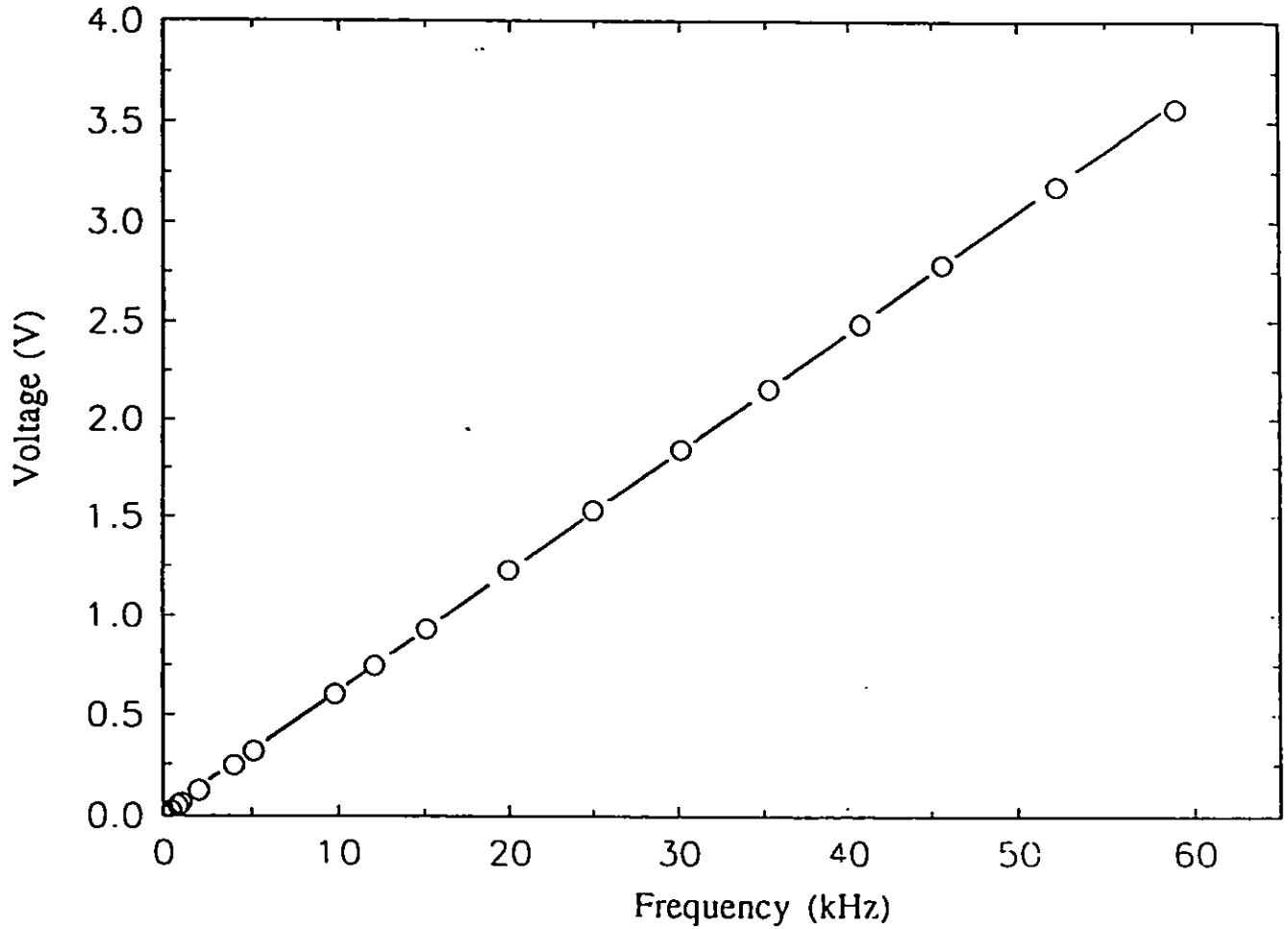

Figure 10. Correlation of the frequency with the voltage obtained from the frequency-to-voltage converter.

deposition of silver on the gold electrode from a solution of 1×10^{-3} M $AgNO_3$ in 0.2M H_2SO_4[3]. 5 μA reduction current (i_R) was employed. The resulting frequency changes on deposition were recorded versus time. The amount of mass deposited was calculated using Faraday's law. For the reduction of silver,

$$Ag^+ + e \rightleftharpoons Ag$$

the charge passed (Q) is given as the product of the plating time (t) and the reduction current (i_R),

$$Q = i_R \times t \qquad (2.1)$$

According to Faraday's law the reduction charge Q can be related to the amount of silver deposited, by the equation

$$m = 107.9\ Q/96486\ (g) \qquad (2.2)$$

where 107.9 is the atomic weight of silver and 96486 (C/mol) is the Faraday's constant. The reduction current and the frequency were recorded

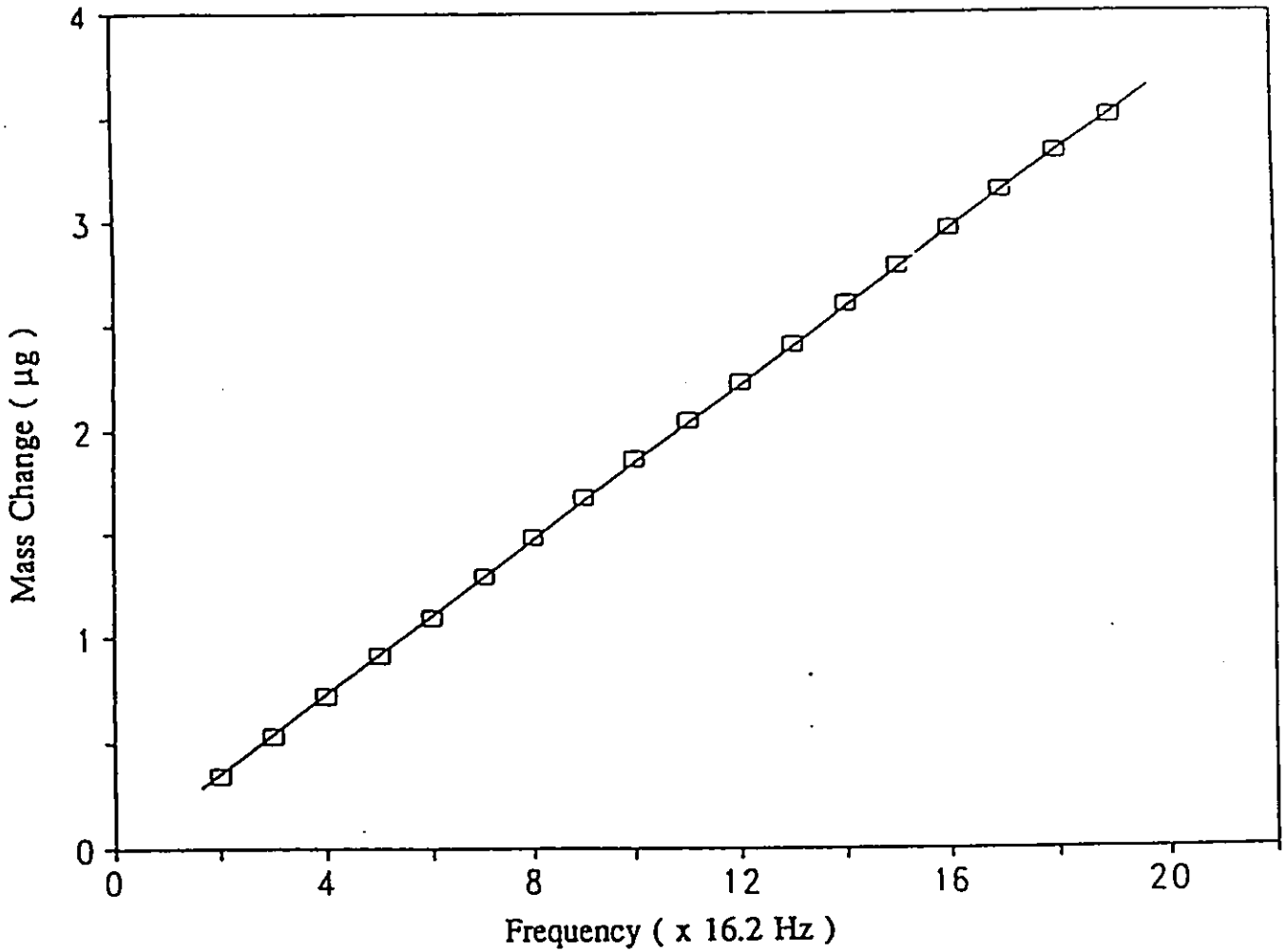

Figure 11. The relationship between mass and frequency for the EQCM.

simultaneously and the relationship between mass and frequency is shown in Figure 11. Considering the geometric surface area of the gold electrode to be 0.25 cm^2, the mass sensitivity of the EQCM is calculated from the slope and was found to be 1.21 ng/Hz which corresponds to 4.4 $ng.Hz^{-1}cm^{-2}$. This agrees very well with the theoretical value of 4.42 $ng.Hz^{-1}cm^{-2}$ calculated from the Sauerbrey equation (1.12) in chapter 1. From the frequency sensitivity (16.2Hz/mV) of the frequency-to-voltage converter, the mass sensitivity of the EQCM is found to be 19.6 ng/mV.

2.5 Chemicals and Solutions.

Solutions were prepared using water from a Millipore Milli-Q purification system. The chemicals Na_2SO_4, Analar; $HClO_4$, Analar and 4,4'-bipyridyl were obtained from BDH and were used without further purification. Ultra pure 99.99% nitrogen (Air Products) was bubbled through the solutions to remove any contamination from oxygen. All the experiments were carried out at room temperature 22 ± 1°C.

CHAPTER 3

RESULTS AND DISCUSSION

(Oxidation of silver in the presence of 4,4'bipyridyl)

The results described in this chapter discuss the oxidation of Ag in the presence of a molecule, 4,4'bipyridyl, which can form a complex with the Ag^+ ion. However before those results are presented it is necessary to describe the oxidation of Ag in the background electrolyte with no bipyridyl present.

3.1 Introduction.

The oxidation of metals in a situation where the metal ion that is produced can then be complexed, either in solution (it may then precipitate) or on the surface is of interest in many practical and analytical applications. In the case of silver, silver halides are important in areas such as photography and in the Ag/AgCl reference electrode system[35]. Such systems have been recently examined with the STM to study the changes in the surface morphology resulting from oxidation-reduction cycles. These

structural changes are of much interest in SERS experiments which produce enhanced SERS signals on surface roughening of electrodes[36,37]. Formation of complexes with metal ions is also relevant to analytical chemistry, for example, complexes are formed between ad-atoms (at the surfaces of copper and silver electrodes) and amino acids and proteins on the electrode surface and these allow protein or amino acid concentrations to be measured with potentiometric methods[38-40]. Another example in analytical chemistry is cathodic stripping voltammetry (CSV)[41,42] where complexes are formed on the electrode surface under controlled conditions followed by a reduction step to measure the amount of accumulated complex. Although Hg is the common electrode material for CSV, silver electrodes have been used in studies of thiouracil and other thioamides[43,44]. The EQCM in conjunction with cyclic voltammetry has also been employed to study the binding of human IgG (Immunoglobulin G) and anti-IgG at a silver electrode[45]. The antibody is strongly adsorbed (at pH 7) and forms an insoluble precipitate at the electrode upon oxidation of silver and the EQCM was found to be suitable for qualitative studies of adsorption of these large molecular structures at a metal-electrolyte interface. Finally, surface complexes are also important in corrosion chemistry, benzotriazole (BTA) has been used as a corrosion inhibitor for Cu and Cu-Zn alloys[46,47] and is thought to function

through complex formation (Cu(I)BTAH). In this thesis the EQCM has been employed in the study of corrosion of Ag electrodes and the subsequent formation of complexes with 4,4'bipyridyl in neutral solutions of 0.1M Na_2SO_4. This system has been studied before[48-50] and has been of interest for two reasons ; the first being that the adsorbed or complexed bipyridyl promotes the reversible electrochemistry of cytochrome c[49] and the second is that Ag is known to be a SERS active substrate and the SERS enhancement is found to be greater when Ag ad-atoms form complexes with the adsorbate. Earlier studies using the SERS technique have shown that when Ag is anodised in the presence of 4,4'bipyridyl a complex (Ag(I)Bpy)[49,50] is formed on the surface of the electrode. In this work the EQCM is used to study the oxidation of silver and the complexation with Bpy in solution and in particular to study the effect of the local concentrations of silver ions and 4,4'bipyridyl on complex formation.

3.2 Oxidation of silver in the background electrolyte.

The background electrolyte used in this study was 0.1M Na_2SO_4. A typical cyclic voltammogram and the accompanying mass response for the oxidation of Ag in 0.1M Na_2SO_4 are shown in Figure 12. The potential is

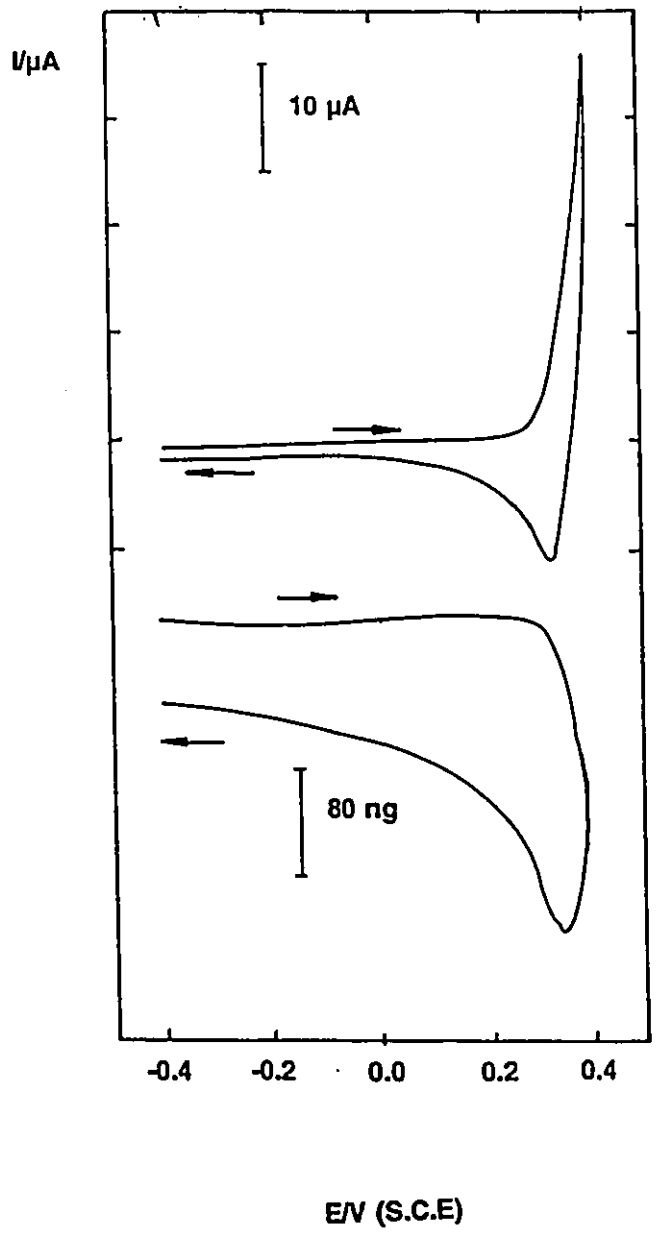

Figure 12. Cyclic voltammogram (top) and mass response (lower trace) for the oxidation of Ag in 0.1M Na_2SO_4. The scan rate was 20 mV/s.

scanned from -0.4 to +0.4V. In this potential range, the production of Ag^+ is the only oxidation process that takes place in solutions of neutral pH. The possibility of the subsequent formation of Ag_2SO_4 either on the electrode surface or as a precipitate is unlikely due to its high solubility (0.57 g per 100 cm^3 of water at 0°C[51]). From the Figure, we can see that as the potential is scanned in the anodic direction, the current increases significantly from 0.25V onwards until the scan is reversed. This is due to the formation of Ag^+ ions. In the reverse scan a cathodic peak is observed at 0.33V which corresponds to the reduction of the Ag^+ formed on the anodic scan.

The mass response reveals no significant changes during the initial stages of the scan but as the oxidation sets in, there is a sudden decrease in mass due to Ag^+ being released into solution. When the scan is reversed the mass starts to increase as the silver is reduced and redeposited on the electrode surface. In Figure 12, 232 ng of material is lost of which all but 60 ng is recovered at the end of the cycle. Thus there is a net mass loss during each cycle (as revealed by the mass loop which does not close). This is due to the fact that some of the Ag^+ produced diffuses away from the electrode and cannot be reduced. However, at higher scan rates the Ag^+ ions released into the solution do not have sufficient time to escape from the vicinity of the electrode surface before reduction takes place. Thus both the mass loss

and the amount of material recovered at the end of the scan depend on the scan rate and both these quantities are higher for a slower scan than for a faster scan. Finally, if the potential is held for sometime at the end of the scan there is no significant change in mass, indicating that no further changes take place.

When the mass loop for an oxidation-reduction cycle does not close, as in the case in Figure 12, one important factor that should be taken into account is a possible change in surface roughness. An increase in surface roughness at some metal electrodes such as Ag, Cu and Au after oxidation-reduction cycles has been reported both in EQCM[52,53] and STM[54,55] experiments. The roughening of the electrode surface is thought to create a situation where solvent molecules get trapped in the surface cavities formed on roughening. Thus, the mass loop does not close [52,53] as the electrode carries more mass at the end of the cycle (the cross sectional view of a simplified roughness model which illustrates this explanation is given in Figure 13[52]). In these examples given in the literature the roughness of the electrodes changes considerably after the oxidation-reduction cycle because an oxide was formed and reduced and the electrodes were either evaporated films or single crystals with low roughness factors. However, in our experiments the product is not an oxide but is the metal ion which is reduced

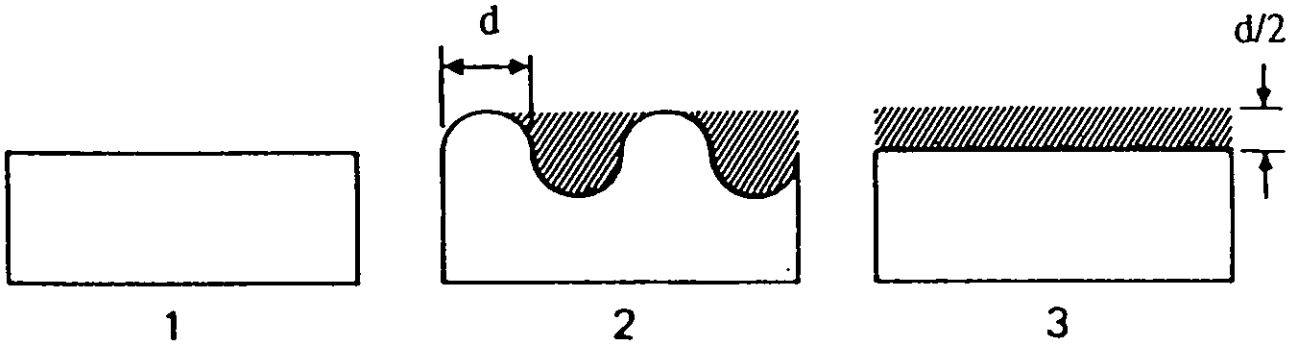

Figure 13. The cross section view of a simplified roughness model[36].

(1) smooth surface; (2) roughened surface made up from hemicylinders with liquid enclosures (hatched area); (3) equivalent rigidly attached liquid layer on smooth surface. Note that the mass of the metal electrode itself does not change in sketches 1 - 3.

and thus redeposited in the reverse scan. In addition, in EQCM experiments in this laboratory using electrodeposited Pt electrodes with roughness factors of 15-30 the mass loops are always found to close after each oxidation-reduction cycle. This is because these electrodeposited electrodes are quite rough at the start of the cycle and so the degree of surface roughness does not change considerably on scanning. This should also be the case for the rough electroplated Ag electrodes used in this study. Thus, in conclusion, the overall mass loss for a cycle in Na_2SO_4 is attributed to loss of Ag^+ into solution and not to a change in roughness of the electrode.

3.3 Oxidation of silver in the presence of 0.25mM 4,4'bipyridyl.

In the previous section we have seen that the oxidation of silver in the background electrolyte produced Ag^+ ions, most of which are rereduced in the cathodic scan and deposited on the electrode once again. Having discussed the oxidation of silver in the background electrolyte the effect of the presence of 4,4'bipyridyl is presented here. In this work 4,4'bipyridyl (Bpy) concentrations from 0.25mM to 10 mM were used but results at 0.25mM are presented here first. (The solubility of Bpy in aqueous solutions is quite small, ~12mM).

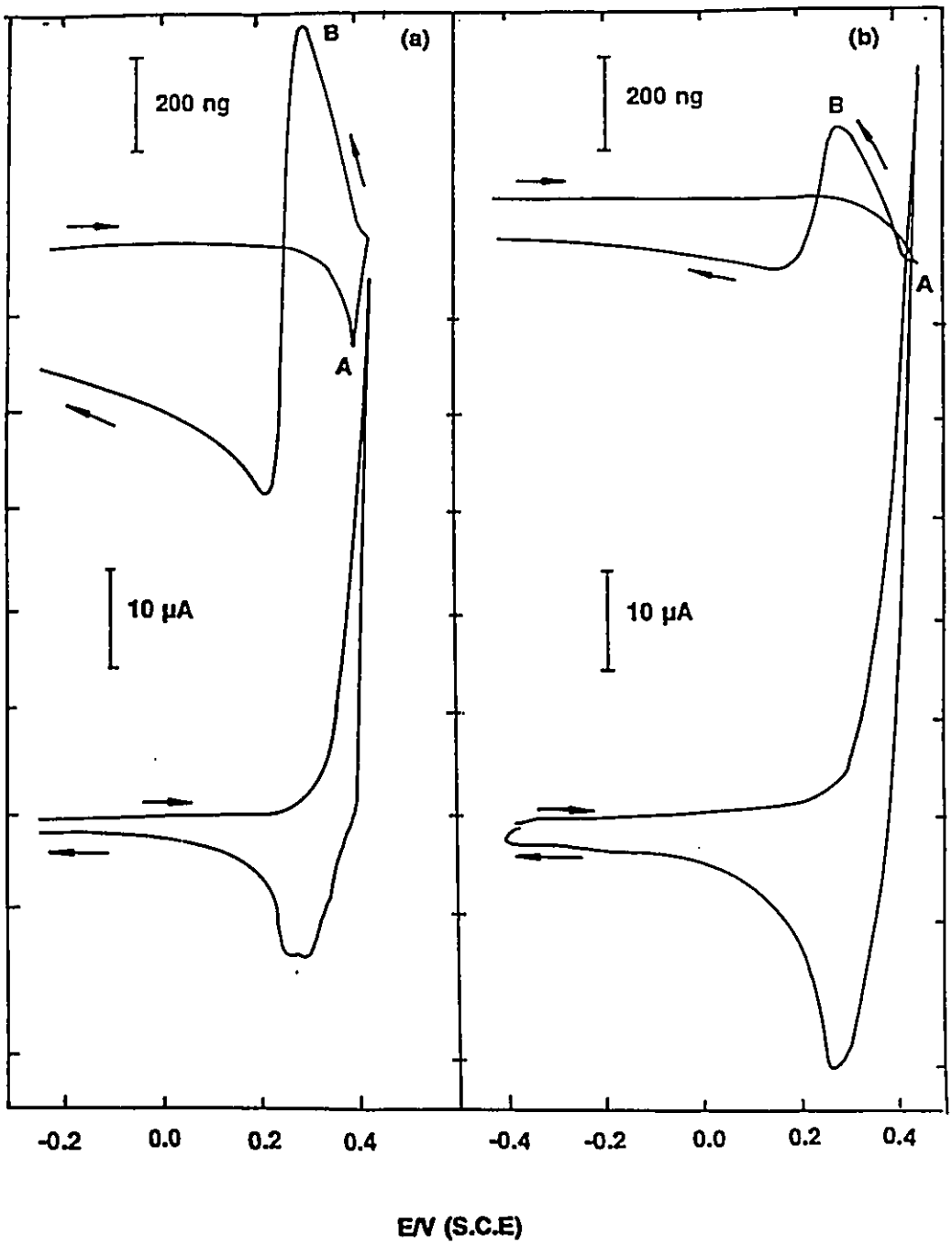

Figure 14. Cyclic voltammograms (lower traces) and mass response (upper traces) for the oxidation of silver in the presence of 0.25mM 4,4'bipyridyl at a scan rate of 10 mV/s (a) and 50 mV/s (b). The upper potential limit was 0.45V as opposed to 0.4V in Figure (12).

Figure 14 shows the cyclic voltammogram and the mass response obtained with a Bpy concentration of 0.25mM for two different scan rates, 50 mV/s (b) and 10 mV/s (a). The upper potential limit was 0.45V. There is not much difference in the voltammetric response at these two scan rates although a broadened reduction peak is observed at the lower scan rate. However, the observed mass changes are substantially different at the two scan rates. At a scan rate of 50 mV/s (b), Ag^+ is released into the solution on the anodic scan and the mass decreases. On reversing the scan the mass starts to increase (indicated by point A) and a peak (B) is observed at which point the overall mass of the electrode has increased relative to its initial value. The mass starts to decrease again when further reduction current is passed. At the end of the cycle there is a net loss of material from the electrode surface. The same type of behaviour is observed at a scan rate of 10 mV/s (a) although the position and magnitude of the features are slightly different. There is an initial loss of Ag^+ as seen in the case of the scan at 50 mV/s, although the point A at which the mass starts to increase is now observed in the positive going scan itself and as the potential is scanned back, peak B is observed again at a potential which corresponds to the maximum reduction current as in the case of the higher scan rate. There is also a net loss of material at the end of the scan as seen in Figure 14 (b).

The results obtained can be explained as due to the formation of a complex between Ag(I) and Bpy followed by its reduction at the surface of the electrode. Similar complexes have been reported from SERS experiments performed under the same conditions as used in our laboratory[49,50], and there are also reports in the inorganic chemistry literature about such complexes with Ag and other metal ions such as Co, Ni, Zn, Cd[56-58] etc.

The mass response in Figure 14 will now be discussed in terms of the effect of complex formation on the results. As the potential is scanned in the anodic direction, the mass responses are initially flat at lower potentials. Then Ag^+ is produced and released into the solution and the mass starts to decrease until point A is reached. If enough Bpy is present in the diffusion layer then Ag^+ may form a complex. This is different from the situation in Figure 12 where there was no Bpy present and hence complex formation was not possible. Once the complex is formed, it has several possible fates. The Ag(I)-Bpy complex is known to have a low solubility, although no precise data is available in the literature. Thus some of the complex formed initially may be lost into the solution. However, when the solubility level of the complex in the diffusion layer is exceeded it will start precipitating on the electrode surface. This will produce a mass increase which begins at point A. The mass may or may not increase above the initial level (at the start of

the scan) depending on the amount of Ag^+ produced and the fraction of this Ag^+ which complexes with Bpy and then forms a precipitate on the electrode surface. The position of point A depends on the amount of Ag^+ generated and the time scale of the experiment (which is influenced by the scan rate if the potential range is not changed) if the concentration of Bpy is constant. On the cathodic scan at 50 mV/s (Figure 14 (b)) the observed mass increase is presumably due to the precipitation of the complex on the electrode. At a slower scan rate of 10 mV/s the time for which the potential is in a region where Ag^+ is generated is greater. Thus the sharp mass increase which results from the complex formation is seen while the potential is still increasing since more Ag^+ is produced much earlier in the anodic scan. The amount of complex formed at 10 mV/s is larger than at 50 mV/s as indicated by the position of point B which represents the net gain in mass from the starting point. When the potential is scanned back the increase in mass continues for a short time as Ag^+ is still released into the solution. This is because the current is still anodic for the initial stages of the cathodic scan. However, when the potential decreases to a value where the complex can be reduced, Bpy is released from the electrode surface and the mass starts to decrease considerably. Although the mass recovers a little (which may be due to further reduction of some free Ag^+ which was present in the diffusion layer)

there is still a net mass loss at the end of the cycle. It is not very clear if the complex is formed on the electrode surface or if it is formed in solution and then precipitates on the electrode. However, the fact that there is a mass decrease due to the release of Ag^+ into the solution before the mass starts to increase due to complex formation suggests that the complex forms through precipitation.

Finally, the structure of the complex on the surface has been suggested by IR spectral data in the literature[56-58]. This suggests that the most appropriate structure is a linear polymeric chain structure in which the 4,4'bipyridyl acts as a bridge between the silver ions (-Ag(I)-Bpy-Ag(I)-). When solid samples of the complex are prepared, nitrate is present to establish the neutrality of charge, in our case this will be achieved by the presence of sulphate.

3.4 The effect of scan rate and potential limits on the oxidation of silver in the presence of 0.25mM 4,4'bipyridyl.

Section 3.3 has shown that the mass response for oxidation of silver with 0.25mM bipyridyl has the same general form at both 10 mV/s and 50 mV/s. This section shows that decreasing the scan rate further below 10

mV/s changes the mass response significantly. Cyclic voltammetry and potential steps are used to gain a better understanding of the processes involved in these changes.

In the previous section, at a scan rate of 10 mV/s in Figure 14 (a) it is seen that in the anodic scan, as the potential reaches its upper limit (0.45V) the rate of mass increase due to complex formation appears to slow down. However, when the scan is reversed the mass increases further as the potential decreases. If the scan rate is lowered to 5 mV/s and the upper potential limit is maintained at 0.45V the mass response becomes more complicated as shown in Figure 15. At this lower scan rate the point A appears much earlier and the mass starts to increase but then decreases at point C. This is apparently the same effect observed at the upper end of the scan at 10 mV/s (Figure 14 (a)) where the rate of increase was seen to slow right at the end of the positive scan. Here at 5 mV/s where more time is spent in a potential region where silver ions are produced, the mass increase not only slows down but actually turns into a decrease. The mass continues to decrease until point D is reached when the mass begins to increase again and leads to peak B. This unusual behaviour could be explained in three ways.

1. The complex formed could be oxidized at potentials above 0.4V.

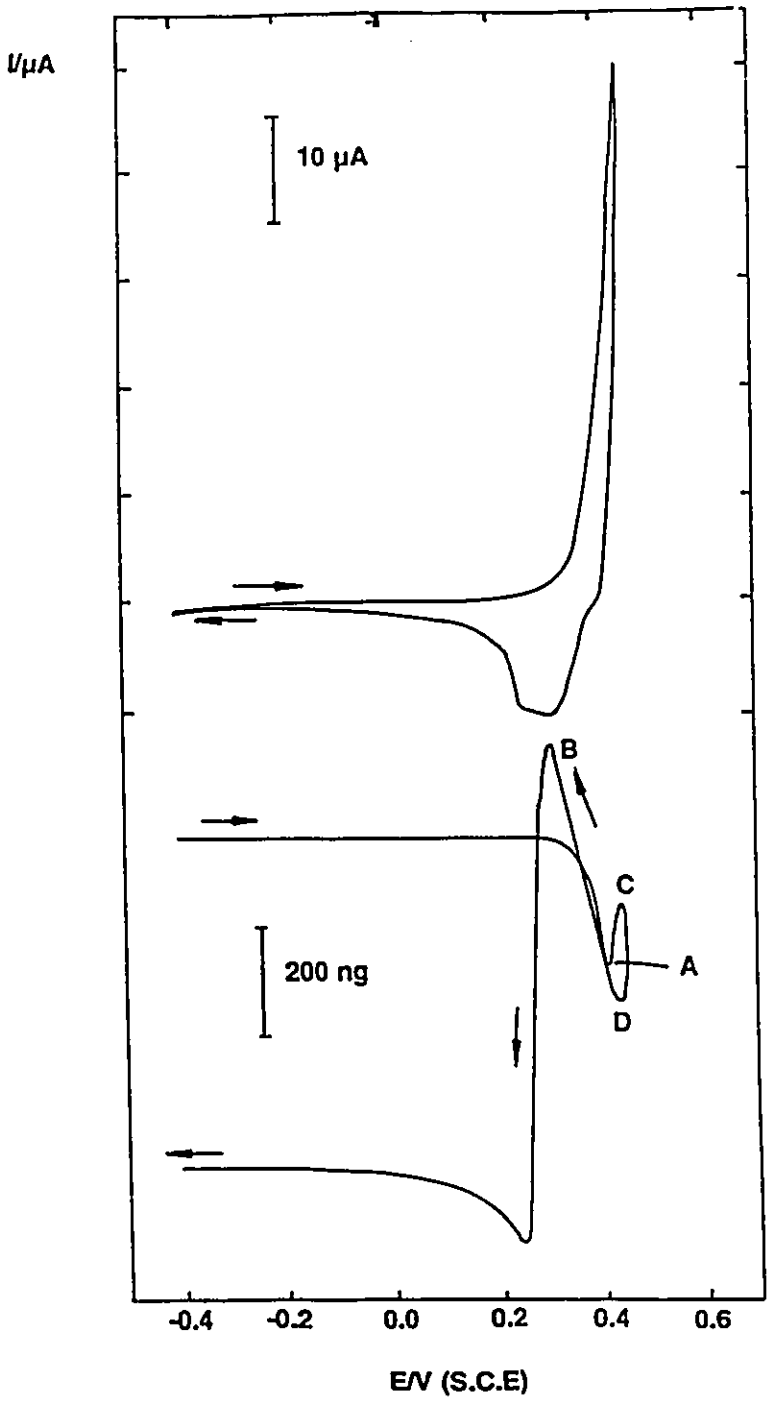

Figure 15. Cyclic voltammogram (top) and mass response (lower trace) for the oxidation of silver in the presence of 0.25mM 4,4'bipyridyl at a scan rate of 5 mV/s. Note that the potential proceeds in the direction A-C-D-B.

However, there seems to be no evidence for this in Figure 14 and the components of the complex are also not easily oxidizable. This explanation seems unlikely.

2. The complex may dissociate. This is also unlikely because more Ag^+ is being produced at the electrode and there is sufficient Bpy in the diffusion layer to allow complex formation to continue.

3. The third possible explanation is that the mass responses observed are due to a balance between two processes. The first is Ag^+ being released into solution (which strongly depends on the potential) which produces a mass decrease. The second contributing process is the formation and precipitation of the complex on the electrode surface which will produce a mass increase. This mass increase will be dependent on the amount of Ag^+ released into solution and the rate at which this Ag^+ is produced and also on the amount of Bpy present in the solution.

If we consider this last explanation to be the most sensible, then point A is not where the complex is first being formed as mentioned before, but it is the point where the rate of mass increase from complex formation exceeds the rate of mass decrease from the dissolution of silver. We can now re-examine the Figures in view of this model of processes at the surface.

For Figures 14 (a) and (b) when the potential is in a region between

points A and B the rate of mass decrease from silver dissolution is smaller than the rate of mass increase due to the complex formation. As a result the mass increases steadily between points A and B. However, at the slower scan rate of 5 mV/s (Figure 15), the balance between the processes controlling the overall mass changes is altered several times. At 5 mV/s more Ag^+ is formed compared to the situation at a faster scan rate, as the potential spends more time in the region where Ag^+ is formed and the rate of formation of the ion will be larger as the upper potential limit (0.45V) is reached. Some of the Ag^+ released into solution is not precipitated (as inferred from the mass signal) and we see a mass loss from C to D because of the fact that, in this region, the mass loss from the escape of Ag^+ will be greater than the mass gain from the precipitation of the complex. However, upon scan reversal the rate of production of Ag^+ is slowed down as the oxidation current is decreased, complex formation dominates the mass change and so a mass increase is seen from D to B. Complex formation is the dominant contribution here as although free silver ion is still present in solution and it may be precipitated, fewer new ions are being generated. The increase in mass continues until the potential decreases to a point where the complex can be reduced. Once this occurs, then the complexed Bpy at the electrode surface is released into solution producing the mass loss seen after point B.

As the potential proceeds further negative then free Ag^+ present in the diffusion layer also becomes reduced and so there is a small gain in mass during the last stages of the cycle. Thus the observed mass change shows how factors such as potential and scan rate, which change the flux and total amount of Ag^+ generated, influence the processes occuring at the electrode surface.

The model presented above is reinforced by the results of potential step experiments. In cyclic voltammetry, the changing potential influences the rate of silver production, causing it to increase and then to decrease during a cycle. A potential step experiment allows this variable to be removed, as the potential is held at a point where Ag^+ is produced continually. The mass response is then observed as a function of time.

Figure 16 shows the mass response due to double potential steps from -0.4V to +0.45V (a) and to +0.4V (b). In Figure 16 (b) the behaviour is similar to that seen in the cyclic voltammetry. Ag^+ is released into solution initially, and there is a mass loss and as the complex formation commences the mass begins to increase and continues until the potential is stepped back. This experiment shows that at 0.4V the mass gain from complex formation is dominant. However when the upper potential was shifted to 0.45V (Figure 16(a)) the rate of Ag^+ production is increased and this changes the mass

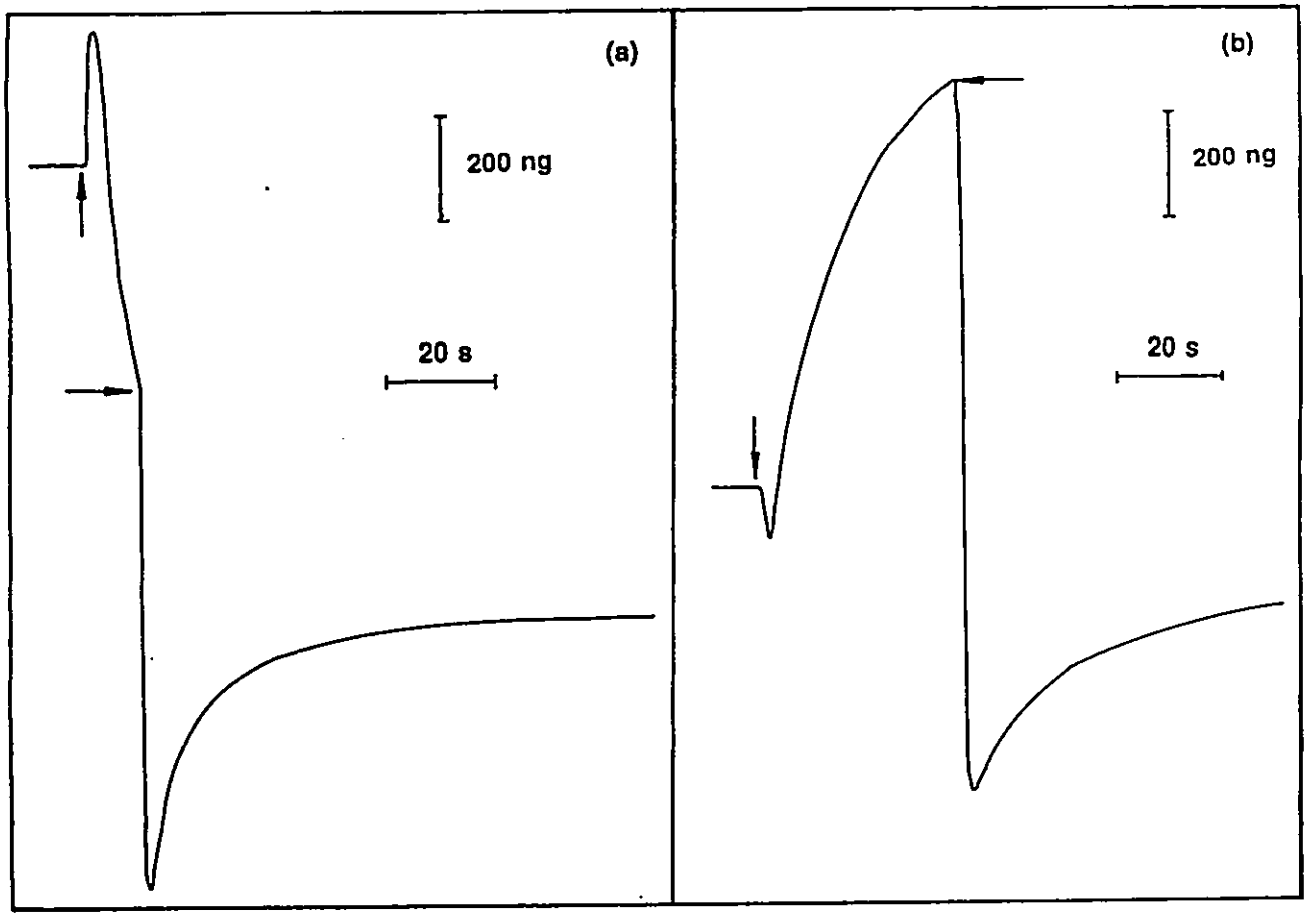

Figure 16. Mass responses resulting from double potential steps between -0.4V and 0.45V (a) and between -0.4V and 0.4V (b). The starting potential was -0.4V and the arrows indicate the points at which the potential steps took place. The solution was 0.1M Na_2SO_4 containing 0.25mM Bpy.

response. Immediately upon changing the potential, the mass increases. Although loss of silver is likely to be faster than at 0.4V, complex formation seems to be dominant at the start. However, within a few seconds, in contrast to Figure 16 (b), the mass starts to decrease and this continues for a few more seconds even after the potential is stepped back to its initial value of -0.4V (at the point indicated by the horizontal arrow). Although complex formation is initially dominant at 0.45V this situation holds good for a very short time. Then the dominant process is reversed as the supply of Bpy by diffusion (after it is initially depleted by complexation) cannot compete with the production of Ag^+ which is much greater at the higher potential. When the potential is reversed to -0.4V a substantial amount of mass is lost. This suggests that in the potential region where Ag^+ is released into solution the observed mass response is a balance between the loss due to Ag^+ and the gain due to the formation of the complex at the electrode surface. Thus even though a decrease in mass is observed when the potential is stepped to 0.45V the complex is still being formed on the surface at a rate which is not sufficient to compensate the mass loss due to the corrosion of the electrode. Reduction of the complex occurs when the potential is stepped back to -0.4V and Bpy which was previously complexed is released into solution which accounts for the further loss in mass seen in Figure 16 (a). Finally, the gain

in mass when the potential is at -0.4V can then be attributed to a contribution from the free Ag^+ present in the diffusion layer which is reduced and redeposited on the electrode. It is likely that the mass change at -0.4V is also a balance of two processes, the first being loss of Bpy after complex reduction and the second being reduction of free silver ions.

3.5 Oxidation of silver in the presence of 2mM 4,4'bipyridyl.

Having discussed the effect of 0.25mM Bpy on the oxidation of silver, the results obtained for the oxidation of silver in the presence of a higher concentration of Bpy (2mM) will be presented here. Earlier we have seen in the cyclic voltammetry in solutions of 0.25mM Bpy that Ag^+ is being produced and released into solution in the anodic scan and after the complex formation with the bipyridyl present in the diffusion layer there is still some free Ag^+ present. The unusual mass responses observed earlier are due to the delicate balance between the two sources of mass changes, namely loss of silver ions into solution and precipitation of the complex at the electrode surface. In these experiments the amount of silver ion produced is affected by the potential but the amount of bipyridyl present is unchanged. This section deals with results where an increased amount of Bpy is present.

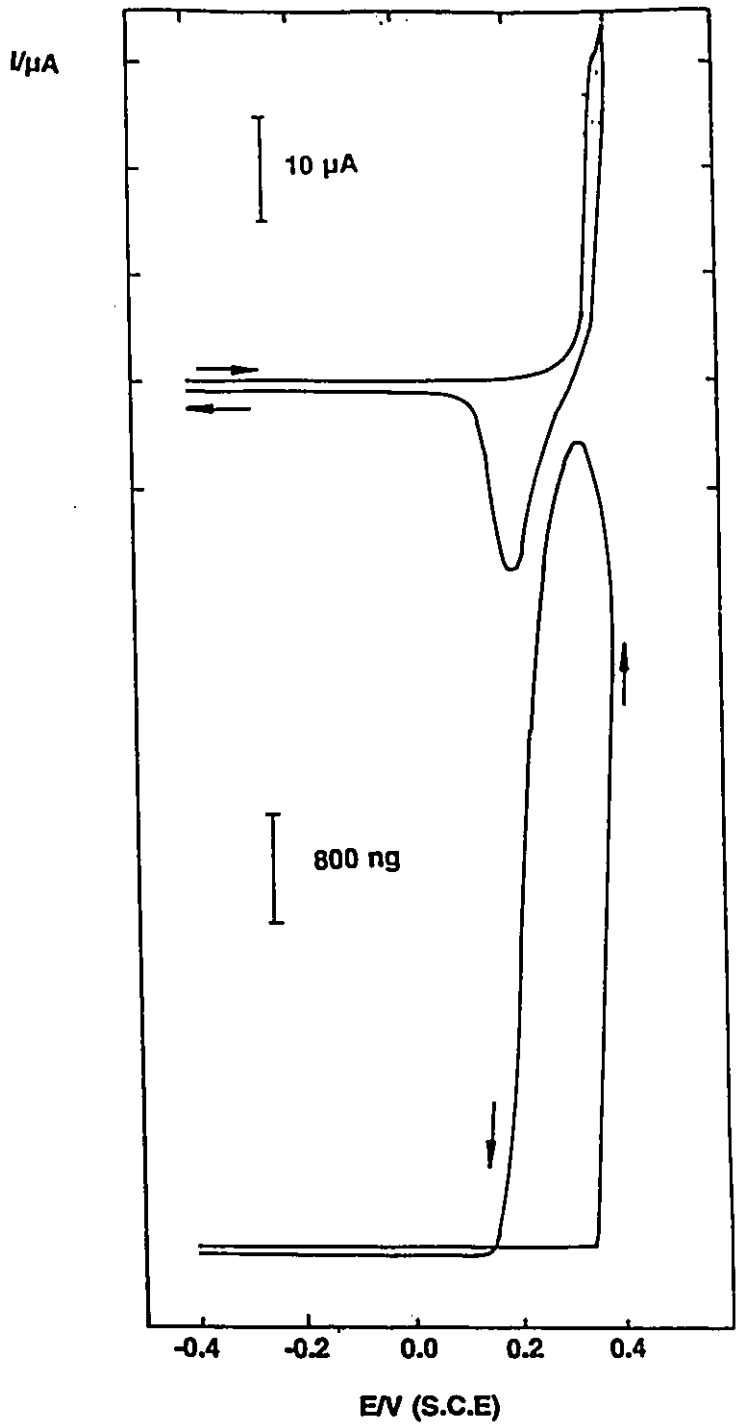

Figure 17. Cyclic voltammogram (top) and mass response (lower trace) for the oxidation of Ag in 0.1M Na_2SO_4 containing 2mM 4,4'bipyridyl. The scan rate was 10 mV/s and the upper potential limit was restricted to 0.4V.

The behaviour at 2mM Bpy is shown in Figure 17 where the upper potential limit is 0.4V. This is much simpler than the mass responses discussed earlier but there are some differences. For example, in the cyclic voltammogram a shoulder is observed which was not seen in the earlier cases. This shoulder can be resolved into a clear peak by increasing the concentration of Bpy (as reported by others[49]) or by decreasing the scan rate (results not shown). Now turning to the mass response, it is initially flat until the Ag dissolution begins when the mass increases sharply due to complex formation with Bpy, then the mass starts to decrease when the complex is reduced on the cathodic scan. The higher concentration of Bpy (2mM) present in this situation makes the mass gain due to the precipitation of the complex the dominant process. By calculating the mass difference between the initial (at the start of the scan) and the maximum value it is seen that 0.59 μg of material is accumulated on the electrode surface. If a 1:1 ratio is assumed for Ag^+ : Bpy, then 2.2 nmol of complex are formed. This is only an estimated figure assuming that all the Ag^+ produced is complexed and that there is no sulphate counterion incorporated into the deposit. Although in the Figure it may appear that the mass signal is quite similar at the beginning and at the end of the scan it should be noted that the mass scale is very large. In fact there is a net loss of material from the electrode surface,

although this loss is only a small fraction compared to the overall mass change observed. These cyclic voltammetric and mass results show that if the Bpy concentration is increased from 0.25mM to 2.0mM then the mass responses are simplified and are dominated by accumulation of complex on the electrode surface. The following paragraphs will show that extending the potential to higher values introduces further complications.

When the upper potential limit is increased to 0.5V in Figure 18, two differences are clearly observed in the voltammogram, when it is compared to that in Figure 17. The first is that after the appearance of the shoulder in the anodic scan an increase in current is seen. The second is the appearance of two reduction peaks in the reverse scan. The shoulder is most likely due to the formation of the complex where the removal of Ag^+ is stimulated at a slightly lower potential than in the case where there is no Bpy present (this is clearly seen in Figure 1 of reference 40). The shoulder may correspond to a situation where the surface concentration of Bpy is reduced to near zero. The sharp rise in current after the shoulder corresponds to faster corrosion of the electrode as much of the Ag^+ released into solution is not complexed.

As in the earlier cases the mass response reveals more information regarding the processes that take place on the electrode surface than the voltammograms. Thus in Figure 18 the mass response is flat at the beginning

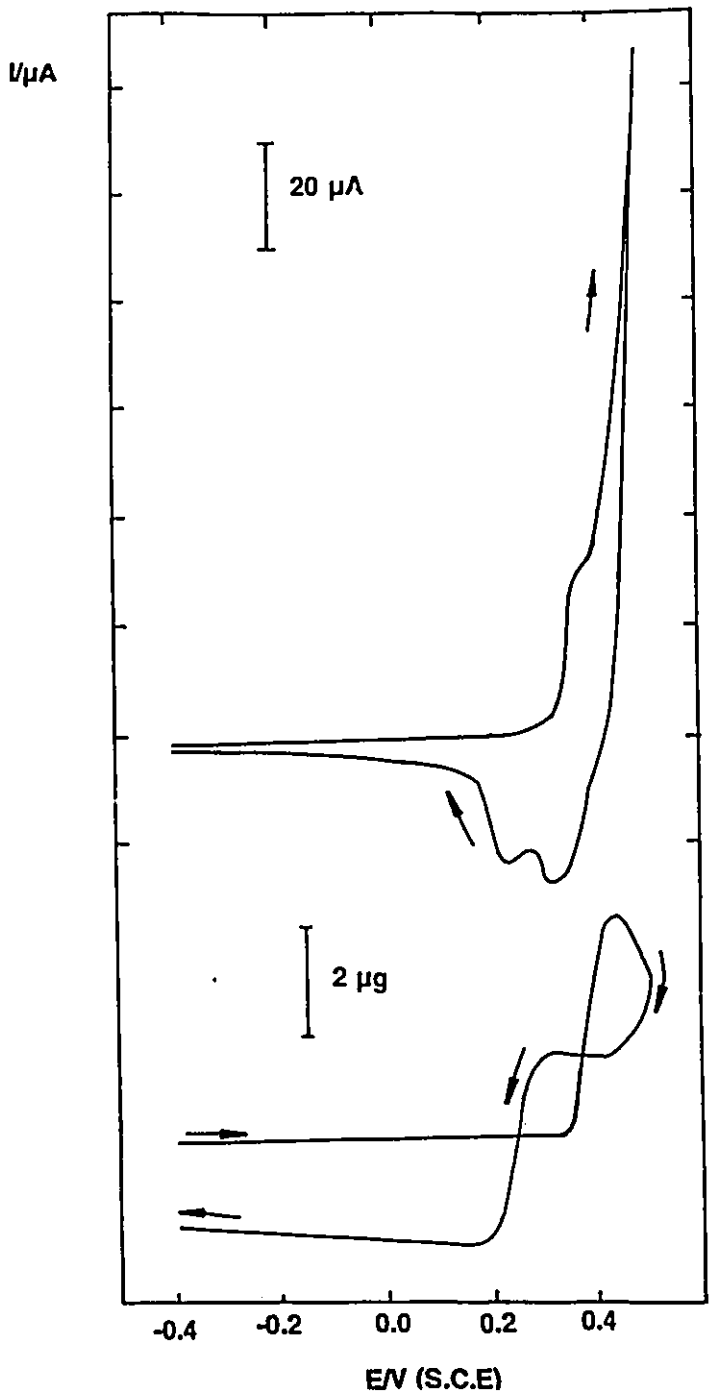

Figure 18. Cyclic voltammogram (top) and mass response (lower trace) for the oxidation of Ag in 0.1M Na_2SO_4 containing 2mM 4,4'bipyridyl. The scan rate was 10 mV/s and the upper potential limit was 0.5V.

of the anodic scan until silver oxidation begins and the ions form a complex with the Bpy. Then the mass starts to increase as in Figure 17, but with the upper potential limit in this experiment being 0.5V there is more dissolution of silver, particularly when the potential is close to the upper voltage limit, and the mass loss thus observed exceeds the mass gain from the precipitation of the complex on the electrode. As a result, the mass starts to decrease as the upper scan limit is reached. When the potential scan direction is reversed and the current drops there is a continued decrease in mass but then a plateau is observed which is coincident with the most positive cathodic peak at 0.33V. It has been reported in the literature that both the cathodic peaks may be due to complex reduction[49] and a pulse voltammetric study of AgCl reduction also found two peaks that were related to two different forms of AgCl deposit[59]. Thus by analogy, we might suggest that two forms of the Ag(I)-Bpy complex are formed. However, because the most positive cathodic peak appears at a value which is close to that of the cathodic peak (0.33V) in Figure 12 and there is no large mass change (on the scale used) associated with it, it is likely that this peak is actually associated with the reduction of Ag^+. Close inspection of the mass signal reveals a very small increase in mass in the plateau region. This increase is estimated to be about 150 ng (with a substantial error involved) which would correspond to 1.4 nmol of

Ag^+ reduced with 134 μC of charge passed. Bearing in mind the error involved, this value is not inconsistent with the results obtained.

Regarding the more cathodic second peak, the mass response that accompanies it is a sharp decrease (Figure 18) which may correspond to the reduction of the complex followed by the loss of Bpy into solution. Finally at the end of the scan there is a big mass loss compared to the start of the cycle which may be caused by the slower scan rate employed and the higher potential limit (0.5V) which would allow most of the free Ag^+ to escape into solution before it can be redeposited on the electrode by reduction. Thus in Figure 18 the two cathodic peaks are clearly identified and this leads us to the suggestion that the broadening of the peak observed in Figure 15 is due to the overlap of the two reduction processes as explained here. Thus in conclusion we can say that, even with a higher concentration of Bpy, when the potential is extended far enough in the positive direction silver dissolution is stimulated and the surface concentration of Bpy is significantly depleted and the resulting observed mass change is mainly due to the corrosion of the electrode.

3.6 Conclusions.

In this chapter we have seen how EQCM and cyclic voltammetry can be used to provide information about the dissolution of silver and its subsequent complexation with Bpy. The delicate balance between these two processes depends on several factors such as the bulk bipyridyl concentration, the scan rate and the upper potential limit. Even though the cyclic voltammetry does not seem to reveal much information, the mass responses provide a clear picture of the different processes taking place at the electrode surface.

When the concentration of Bpy is low (0.25mM), not all the Ag^+ produced is complexed and then the rate of mass decrease due to Ag^+ is the dominant process at first until the mass gain due to complex formation takes over at point A (Figures 14 and 15). When slower scan rates are employed the point A shifts to more negative potentials because more Ag^+ is released into the diffusion layer at a given potential. An increase in scan rate (10 mV/s, Figure 14 (a)) along with an increase in the upper potential limit (0.45V) will result in the dominant process in the mass change being complex formation on the electrode surface. When the scan rate is lowered to 5 mV/s the balance between the processes switches twice as shown in Figure 15 even before the complex is finally reduced.

When the concentration of Bpy is increased to 2mM the dominant

process in the mass response is due to the formation of the complex because of the larger amount of Bpy present. The observed mass response is very simple, first a large mass increase is seen due to the accumulation of the complex on the electrode surface and then a mass loss when this complex is removed by reduction. If the potential is extended further positive (0.5V) the concentration of Bpy is depleted and then more silver dissolution takes place and the mass decreases consequently. Then on the reverse (cathodic) scan two reduction peaks are observed of which the first one is considered to be due to the reduction of Ag^+ and the second one due to complex reduction.

In conclusion, the corrosion of the electrode and the complexation at the electrode surface has been investigated by combined cyclic voltammetric and mass measurements. The results obtained show the advantages that the mass measurement brings to the study of electrode processes as the EQCM response is much more informative than the voltammograms.

CHAPTER 4

RESULTS AND DISCUSSION

(Reduction of 4,4'bipyridyl at silver electrodes)

4.1 Introduction.

There have not been many studies of the electrochemistry of 4,4' bipyridyl (Bpy) but most have been at Hg[60-63] or Au electrodes[64-66]. At gold, the interest was stimulated because Bpy was the first compound found to act as a promoter for the redox protein cytochrome c[67]. Thus, when adsorbed at a gold electrode, Bpy prevents the denaturation of the protein and allows electron transfer to take place while also preventing the protein from losing its structure. Bpy itself does not undergo any electrochemical change during this process. Bpy was also found to act as a promoter for cytochrome c at silver electrodes and this led to some Raman and SERS studies of this system[48-50]. These SERS studies of Bpy at Ag revealed several interesting features including film formation upon reduction, adsorption of Bpy in neutral solutions and adsorption of doubly protonated Bpy in acid solutions through ion-pairing with halides at the electrode surface[48-50]. These features

of the Ag-Bpy system make it an interesting test of the ability of the EQCM to probe different aspects of adsorption at electrodes.

4.2 Electrochemistry of 4,4'bipyridyl.

A short review of the reduction of Bpy is presented here first. The processes seen depend on factors such as pH and concentration and the anion in the electrolyte[68]. Unprotonated 4,4' bipyridyl has three equivalent redox states - Bpy, $Bpy^{-\cdot}$ and Bpy^{2-}. Below pH 6, Bpy is protonated (pK_A values are 3.5 and 4.9 for the first and second protonations respectively[57]) and at Hg electrodes the doubly protonated species ($BpyH_2^{2+}$) is reduced twice in one electron steps[61,62]. In strong acid solutions, the second reduction process occurs at a potential more negative than hydrogen evolution but as the pH is increased to about 3.5 and hydrogen evolution shifts towards more negative potentials the second reduction can be observed. At solid electrodes (Ag or glassy carbon) work suggests that the reduction changes to a two electron process above pH 6 and gives the dihydrobipyridyl, H_2Bpy[50]. The two electron reduction product, or a product derived from it complicates the electrochemical response in solutions of neutral pH, but this effect is only seen at low concentrations. At a glassy carbon electrode in 0.1M KCl with

1mM Bpy the reduction process is reversible but if 10mM Bpy is used the peaks in the voltammogram move further apart and the electrochemistry becomes irreversible. This has been attributed to a blocking (inactive) film of $BpyH_2$ that may be a polymer[50]. The inactivation process is believed to be too slow to compete with the re-oxidation when Bpy concentration is low. Finally, chloride ions were found to promote the adsorption of Bpy at rough Ag electrodes (i.e. polished silver wires that had then been subjected to a double potential step). Thus in 0.1M KCl, the normal reduction peak is preceded by a peak that is associated with the two electron reduction of adsorbed species. This peak was not observed in 0.1M Na_2SO_4[50].

4.3 Cyclic voltammetry of 4,4'bipyridyl at Ag electrodes.

Figure 19 shows typical voltammograms for the reduction of 2mM Bpy at a silver electrode in 0.1M Na_2SO_4. The potential is taken to two different negative limits at a scan rate of 50mV/s. On the negative scan, two interesting features are observed ; a shoulder (a) at -1.15V and a second peak (b) at -1.35V before hydrogen evolution takes place. In the reverse scan the shoulder (a) corresponds to a sharper peak (a'). It has been suggested earlier by other workers that the first shoulder (a) might be due to a two electron

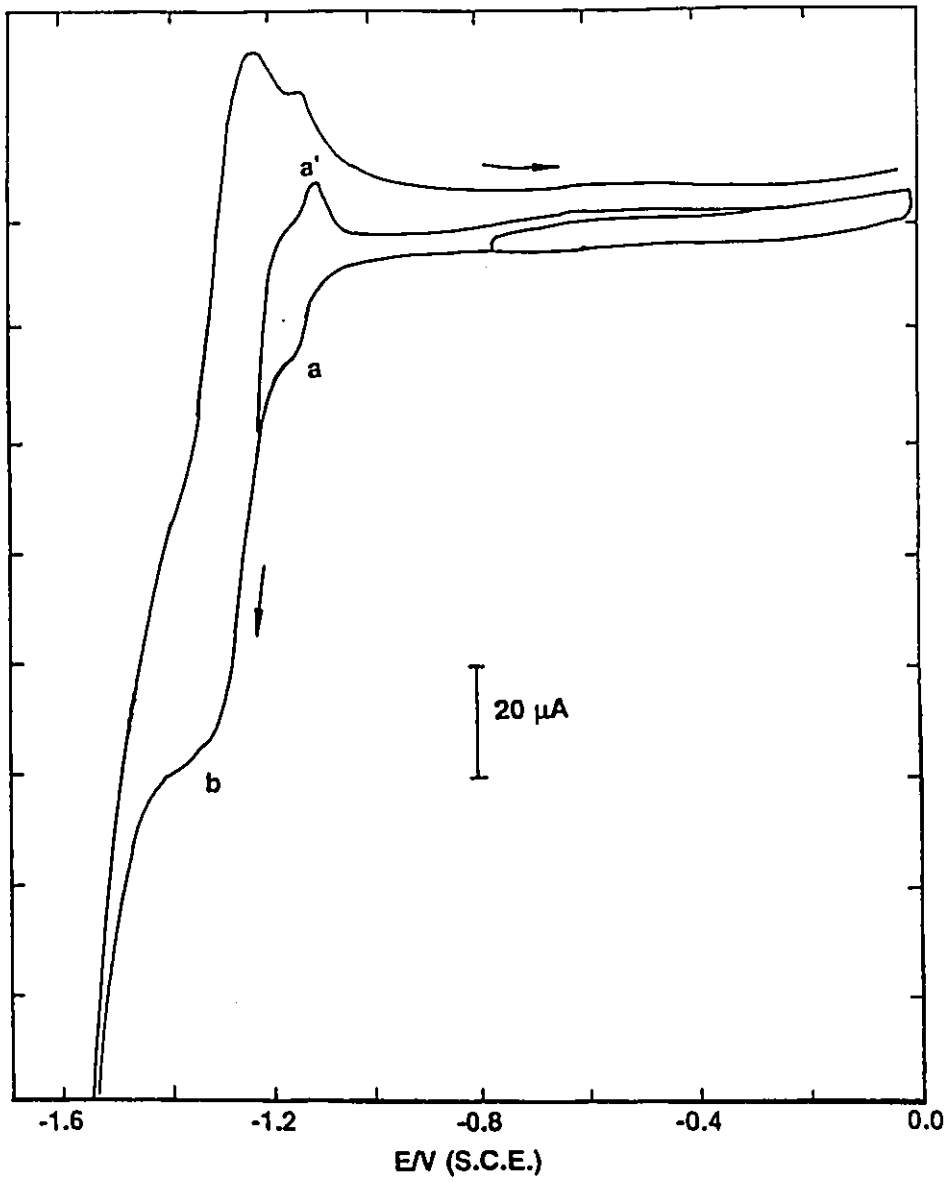

Figure 19. Cyclic voltammograms for the reduction of 2mM Bpy at an electroplated Ag EQCM electrode in 0.1M Na_2SO_4. Scan rate was 50 mV/s.

transfer to adsorbed Bpy. If this was the case we should expect to see a direct dependence of peak height on scan rate. However, in this work the peak observed is less prominent than that reported by others[50] and the electroplated Ag electrodes used here have high charging currents making background subtraction difficult and so it was not possible to verify whether or not peak (a) corresponds to a surface species. However, a potential step experiment to -1.15V produced a current transient which did not decay to zero but a small steady state current (7-8 μA) was produced during the time observed (90s) which suggests that not all the current is due to adsorbed species. It has been reported earlier that the adsorption peak (a) was observed in 0.1M KCl but not in 0.1M Na_2SO_4. The fact that peak (a) is seen here in 0.1M Na_2SO_4 could be due to the difference in the methods of electrode preparation. Electrodeposited silver electrodes were used in this work whereas in the earlier study the electrodes used were polished silver wires that were then roughened in the presence of Bpy since they were to be used for subsequent SERS experiments[50].

After peak (a), a second peak (-1.35V) is observed when the potential is scanned more negatively. (This peak is found to be more pronounced at lower scan rates). Some polarographic studies reported earlier[60-63] suggest that the two electron reduction takes place only at pH higher than 9.

However, the results on silver electrodes show that this two electron reduction is observed at pH ~6. In addition, SERS studies[50] have shown that when the potential is held in the region of this second peak a Raman spectrum is observed which corresponds to a doubly reduced species. This suggests that the second peak at -1.35V corresponds to a two electron reduction of Bpy coupled with the addition of two protons to form $BpyH_2$.

On the anodic scan two peaks are observed followed by a broad oxidation region which stretches up to 0.0V. This is due to the formation of a film on the electrode surface, which will be discussed later. It was found that after every cycle when a film is formed, the electrode had to be cycled between 0.0 and -0.8V several times to restore the background current to its original level. This was found to be very important for reproducible electrochemistry to be obtained each time the potential was again scanned to the region were film is formed.

4.4 Cyclic voltammetry and mass responses - Film formation on reduction.

In the previous section the electrochemistry of the reduction of Bpy was discussed. Here the cyclic voltammetry and the accompanying mass

response when the potential is scanned to -1.3V is presented (Figure 20). At this potential limit the reduction current is still considered to be due to the reduction of Bpy and not due to hydrogen evolution.

In this solution containing 2mM Bpy the mass response is flat if the negative potential is limited to -1.2V (curve 1). The adsorbed Bpy removes the small changes that are visible when the mass is recorded on the same scale in the background electrolyte alone (background response is not shown here). Earlier studies using electroplated Ag electrodes in different electrolytes[69,70] also showed only very small mass changes with potential. In this work the small changes observed can be attributed to the changes in specific adsorption with potential and are largely removed when adsorbed Bpy is present on the electrode. (A similar effect was observed when Bpy adsorbed on Au[66]). The flat mass response that is observed when the potential is scanned between 0.0 and -1.2V is the "background response" for the rest of the results to be presented in this chapter.

Extending the negative potential limit to -1.3V (curve 2) changes the observed behaviour significantly. At the very end of the negative scan the mass starts to increase slightly and continues to increase during the early stages of the reverse scan until the net current is anodic. At this point the mass starts to decrease and this decrease continues until the end of the scan.

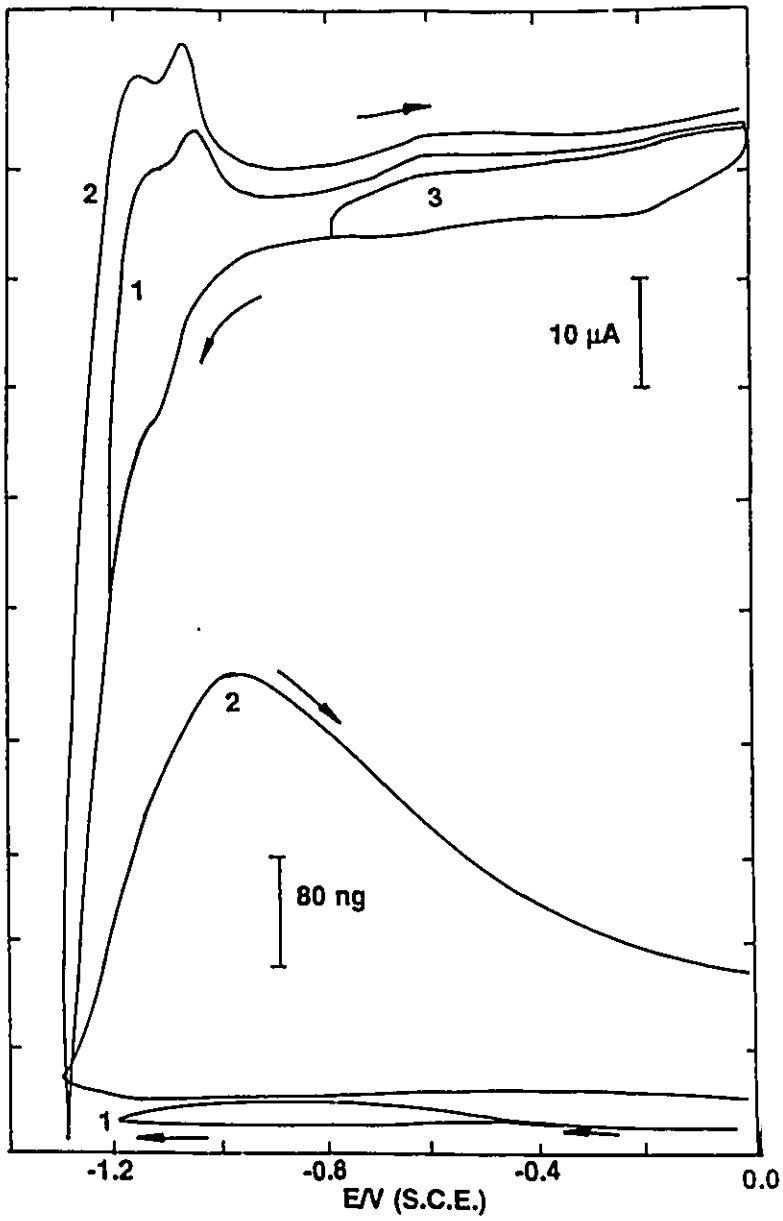

Figure 20. Cyclic voltammetry (top) and mass responses (lower trace) for 2mM Bpy in 0.1M Na_2SO_4 at 50 mV/s.

Potential was reversed at -1.2V on cycle 1 and -1.3V for curve 2. Curve 2 was recorded directly after curve 1. Background current (curve 3) is also shown for an electrode cycled between 0.0 and -0.8V where no reduction of Bpy is seen. Note that the current scale is different from that of Figure 19.

The mass does not return to its original value but this can be attained by cycling the electrode between 0.0 and -0.8V a few times in the same way that was used to obtain reproducible electrochemistry.

The mass response reveals that a film is developed on the electrode when Bpy undergoes reduction and this film continues to grow until the reduced Bpy begins to oxidize in the reverse scan. This is not revealed by the cyclic voltammogram. It is seen that most of the mass increase is during the reverse scan when the reduction current is decreasing which indicates that the film formation begins only when a sufficient amount of reduced Bpy is present on the electrode surface. Although the electrochemistry appears to be reversible, both the current and mass response illustrates that the film removal process is slow.

In Figure 21 the cathodic limit is further extended to the hydrogen evolution region. The Figure illustrates that when the potential limit is extended to -1.6V more charge is passed during each scan and the amount of material deposited on the electrode increases. However, the rate of film growth slows down significantly as hydrogen evolution begins and in fact the mass starts to decrease during the positive scan until the potential is positive enough so that reduction of Bpy resumes and the film starts to grow again. As pointed out earlier, the larger current in the double layer region and the

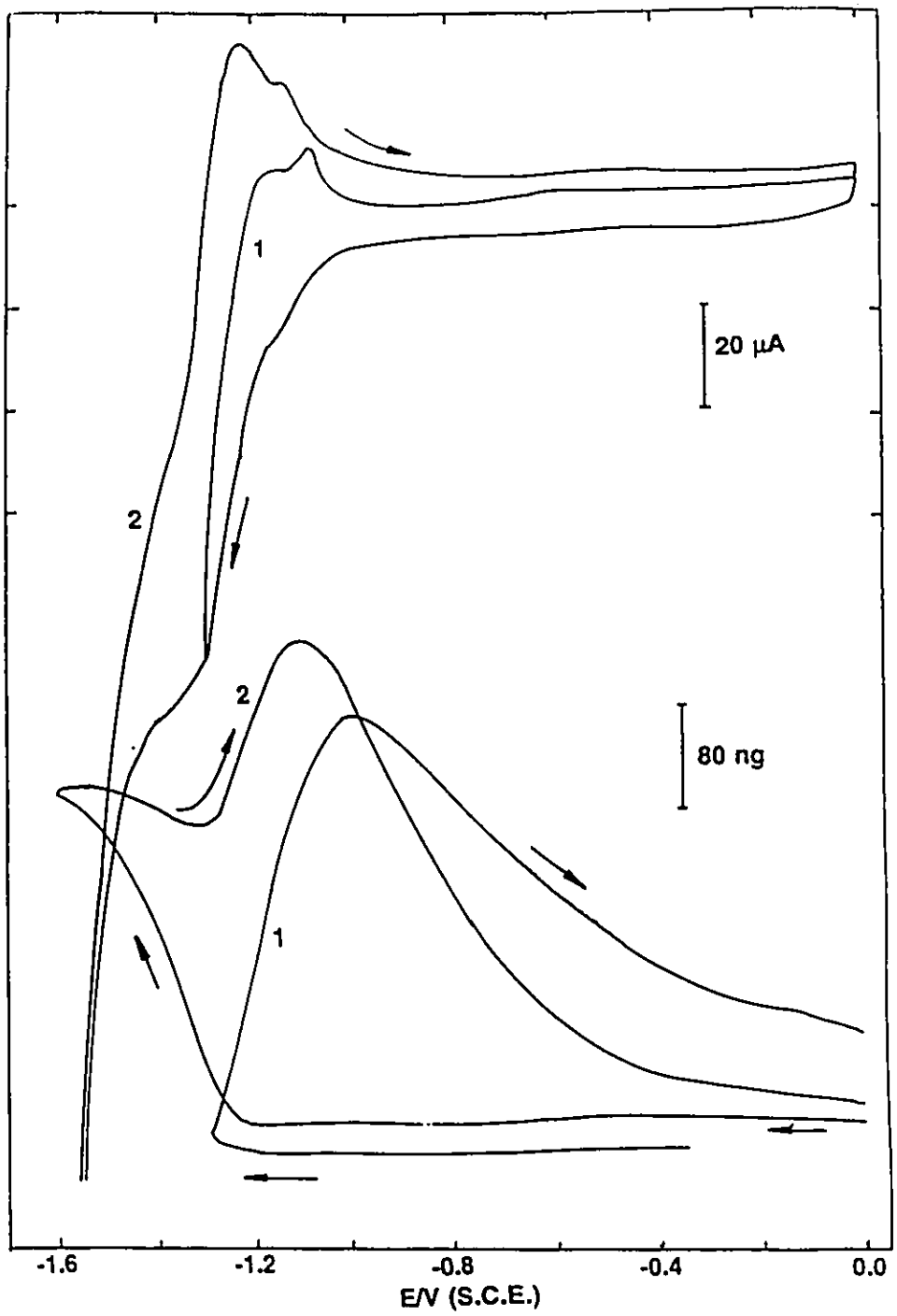

Figure 21. The effect of hydrogen evolution on cyclic voltammograms and mass responses for reduction of 2mM Bpy in 0.1M Na_2SO_4.

Electrode potential was reversed at -1.3V (curve 1) and -1.6V (curve 2). The potential was cycled between 0.0 and -0.8V until a stable background response was obtained before recording each scan. Scan rate was 50 mV/s.

mass response suggests that film removal is slow. Both the mass and current response presented in Figures 20 and 21 could be reproduced by cycling the electrode in the region between 0.0 and -0.8V after every experiment. After this procedure the current would return to its original level and the mass to its starting point. However, after each experiment when the electrode was cycled a number of times in the region were film is formed, the mass of the electrode was found to increase slightly. Thus in conclusion, if the potential is taken sufficiently negative a film is formed on the electrode surface and the rate of film removal process is found to be slow.

4.5 Potential step experiments.

In the previous section we have seen that a film of reduced Bpy develops on the electrode surface at high negative potentials. In order to observe the rate of film growth and its development (including whether the film thickness reaches a limiting value or not) potential step experiments were performed. The potential was either stepped from 0.0V to a final value and then stepped back to zero (double potential steps) or the potential was stepped from 0.0V and then scanned back to zero (single potential step - these experiments are reported in more detail in the next section (4.6)). The

electrode was prepared for each experiment by cycling between 0.0 and -0.8V so that it would be free from any film formed prior to the step.

Figure 22 illustrates the mass responses resulting from the potential steps from 0.0V to -1.15V (b), -1.25V (a) and -1.45V (c). The potential steps to -1.15V (b) and -1.45V (c) resulted in very small mass increases but in the case of the potential step to -1.25V (a) a significant growth of the film was observed (a large mass increase) and the growth lasted for about 90s until the potential was reversed. 3.9 μg or 23 nmol of material (assuming that it is all bipyridyl) was deposited on the electrode surface. It is possible to make a rough estimate of the number of monolayers present at the electrode surface using this figure. However a knowledge of the electrode area is required first. This was estimated by assuming that the roughness factor of the plated Ag electrode is similar to that of plated Pt electrodes prepared in this laboratory, or 16, giving an approximate area of 4 cm^2. However, it should be recognised that this is an estimate only. Using this value for the electrode area we find that 5.8 nmol cm^{-2} of Bpy is present on the electrode. If 0.5 nmol cm^{-2} is considered as a suitable value for a monolayer[49] (0.37 nmol cm^{-2} has been suggested from results at Hg[60]) then about 12 monolayers of reduced Bpy are present at the electrode surface. This value is very approximate and there is a great deal of uncertainty associated with

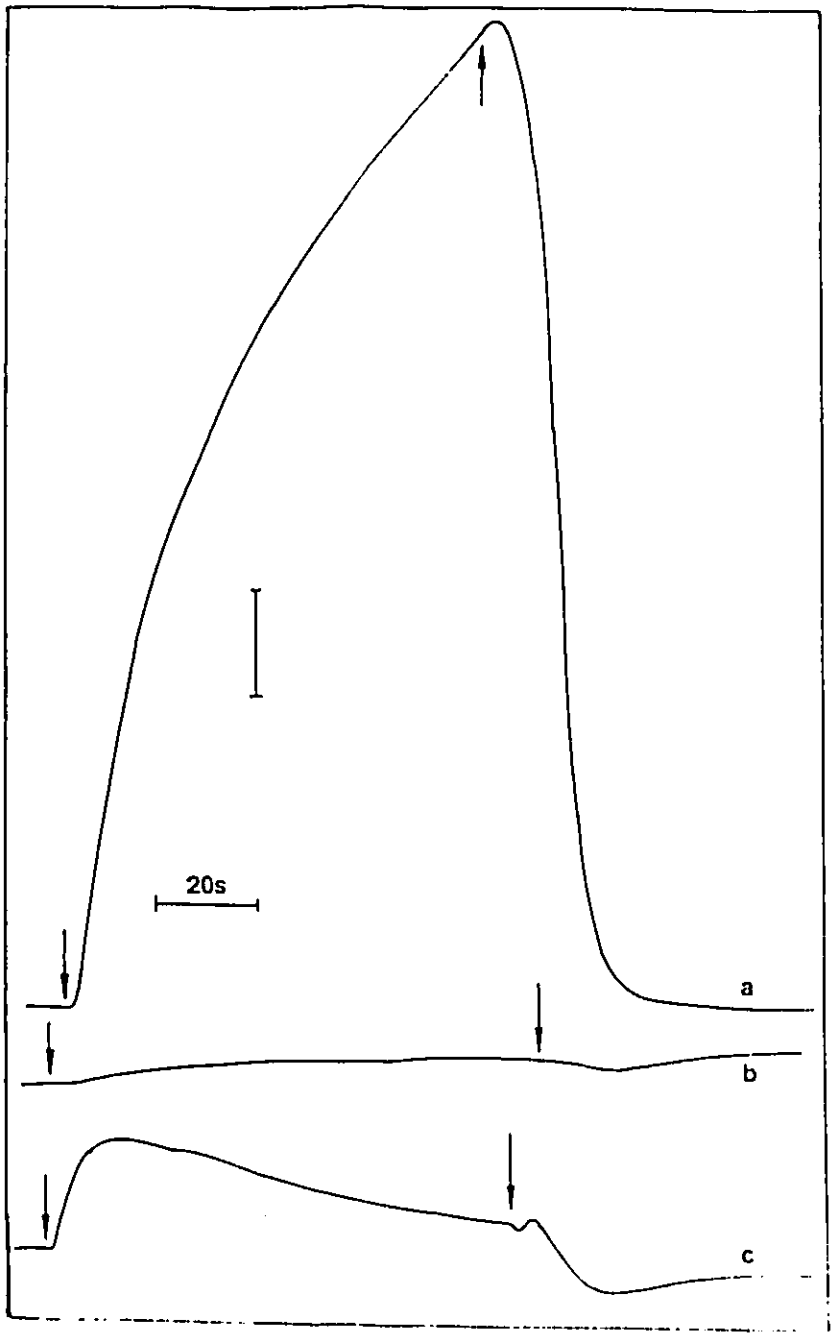

Figure 22. Mass responses accompanying potential steps from a starting value of 0.0V to -1.25V (a), -1.15V (b), and -1.45V (c).

The mass bar is equivalent to 400ng (a), 200ng (b), and 80ng (c). Prior to each step, the electrode was cycled between 0.0 and -0.8V at 50 mV/s to establish complete removal of any previously developed film. For each trace the first vertical arrow indicates the point at which the potential was stepped to the holding value and the second vertical arrow indicates the point at which a scan (50mV/s) back to 0.0V was begun from the holding potential.

this figure. For example, it is quite possible that counter ions (sulphate) and water are incorporated into the film upon formation but without further study it is not possible to make a more accurate calculation.

The mass transient (a) in Figure 22 also shows that the mass increase is not linear with time which suggests that the rate of film formation decreases slightly as it becomes thicker. The reduced Bpy is generated by the electron transfer to solution Bpy and this stimulates the growth of the film on the electrode surface, the presence of the film may inhibit further growth but the data suggest this effect is small over the time scale of this experiment. The mass transients (b) and (c) do not show any significant mass increase due to film formation. In the case of (b) the potential limit (-1.15V) is not negative enough for film formation to occur; a steady state current can be maintained but the product formed may not be the doubly reduced form of Bpy or the amount of reduced Bpy produced may not be sufficient to lead to film formation. On the other hand, when the potential is too negative (-1.45) as in (c), the film formation is probably prevented by hydrogen evolution. This disruption may be a mechanical one where the film formation is blocked by bubble formation due to hydrogen evolution or a complication from a reaction with hydrogen. Polarographic studies by Heyrovský[61] have also suggested (from catalytic currents observed at a dropping Hg electrode)

that if the pH is below 7 the doubly reduced Bpy may react with protons in a catalytic cycle to produce $H_2Bpy^{+\cdot}$ and H atoms. These H atoms may react to form hydrogen or they may hydrogenate the pyridine rings of Bpy. However, there is no evidence of this type of behaviour in our work perhaps because of the (relatively) high concentrations of Bpy used here makes the inactivation reaction of Bpy the dominant process and not the generation of H atoms. In the polarographic work reported [61] very low concentrations (2.0×10^{-5} M) of Bpy were used (as opposed to 2mM used here) and so the generation of H atoms must compete with the inactivation reaction of Bpy.

In summary, the double potential step experiments reported in this section provide an indication of the potential at which film formation occurs on the electrode surface and also allow an approximate calculation of the thickness of the films formed to be made. The next section presents some experiments on the removal of these films by oxidation.

4.6 Re-oxidation of films of reduced Bpy.

We have so far discussed the formation of films on the electrode surface either through cyclic voltammetry or potential steps performed under

appropriate conditions. The amount of material deposited on the electrode can be inferred from the mass response and can be controlled to a good degree of reproducibility by using a potential step to an appropriate potential and then holding the potential for a set time. In this section the re-oxidation of the reduced Bpy films formed on the electrode will be presented.

The re-oxidation process was found to be less reproducible than the reduction and showed many interesting features. From previous results (Figure 20, curve 2), where the potential was scanned to -1.3V at 50 mV/s the voltammetry shows that film removal is not complete at the end of a scan (the current does not return to its starting value) unless only a small amount of material was deposited originally during the negative scan. It is also seen that the mass does not return to its starting value. Clearly under these conditions, film removal is slow. In addition, it was found that when thicker films are formed on the electrode then a new and unusual peak appears in the voltammetry on the positive going scan. This peak is seen in Figure 23 which shows cyclic voltammograms and the accompanying mass responses for two different scan rates (10 mV/s and 50 mV/s) when the negative potenial limit was -1.3V. The reduction chemistry in this Figure is as observed before although in the case of the cyclic voltammogram at 10 mV/s the second reduction peak is more pronounced than in the case of a

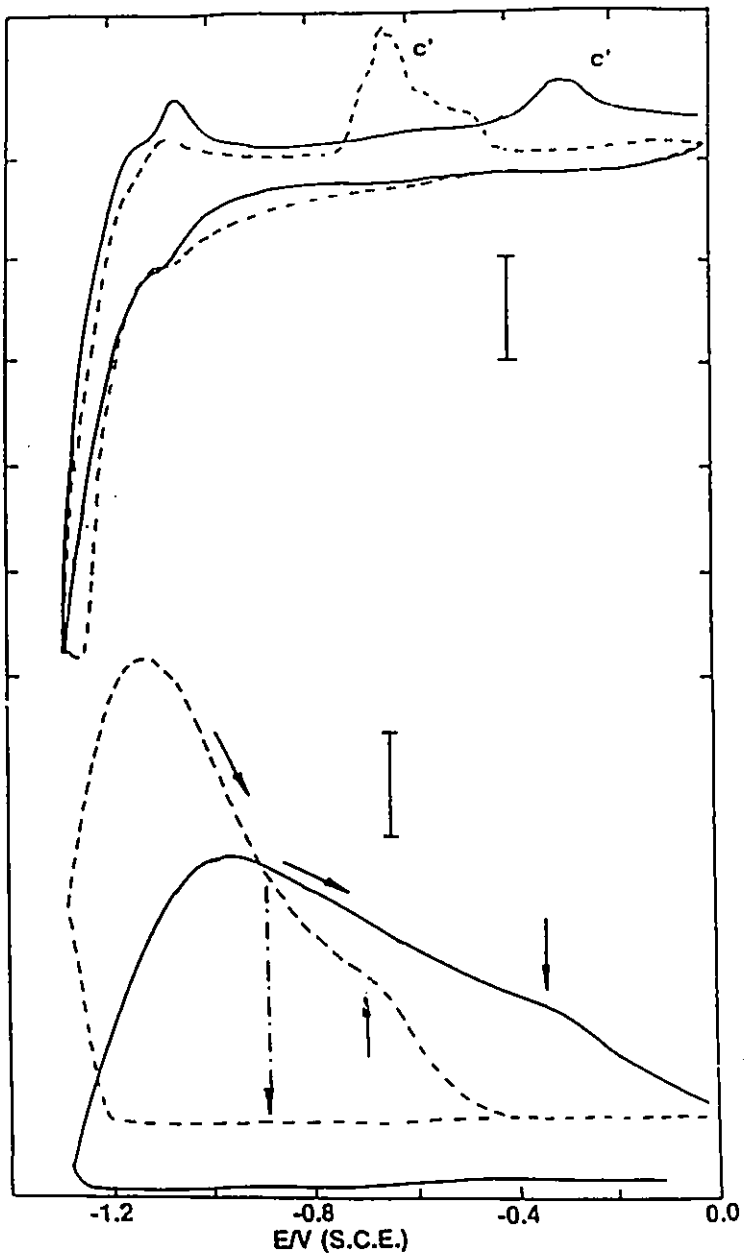

Figure 23. Cyclic voltammograms and mass responses for the reduction of 2mM Bpy in 0.1M Na_2SO_4 at two different scan rates, 10mV/s (dotted line) and 50mV/s (solid line).

The current bar is equal to 5 μA (10mV/s) and 10 μA (50mV/s). The mass bar is equal to 400ng (10mV/s) and 200ng (50mV/s). The solid vertical arrows indicate the point where the slope of the mass response changes while the dotted vertical arrow is a schematic illustration of the way in which the mass decays to its starting value if the potential is held at -0.9V after a film has been developed on the electrode.

faster scan rate (50 mV/s). It is in the return scan back to 0.0V that the new peak (c') which has an uneven noisy structure is seen and the position of this peak depends on the scan rate, occuring at a more positive potential at a faster scan rate. A similar peak was reported earlier in the literature and was considered to be due to the formation of the cation radical $BpyH_2^{+\cdot}$.This cation radical is coloured and a purple species was reported to be observed streaming away from the cathode[50] as the potential passed through the region of this peak. Another interesting phenomenon observed was that the rise in current that led to this peak also produced a change in the slope of mass decrease (as indicated by the vertical arrows in the Figure). Thus a more rapid removal of mass takes place from the electrode surface on the onset of the peak (c'). However, the mass of the electrode does not return to its initial value in this experiment.

When the experimental data were inspected, the data indicated that the peak c' and the increase in the rate of mass removal that was triggered on the onset of the peak were characteristic of experiments where thicker films were formed on the electrode surface. Several other experiments were performed to investigate the nature of the process that leads to this peak c'. Preliminary results showed that the onset of the peak and the rate of change in the slope of the mass occurred at a point that was approximately at the same distance

from the starting mass, suggesting that the peak may correspond to the removal of the last layer or several layers of Bpy. In order to test this, the potential was then scanned to -1.3V and held for some time to grow a thicker film on the electrode (monitored by the increase in mass) and then the scan was reversed to 0.0V. The reverse scan showed a peak and a change in the rate of mass decrease that occured at much higher levels of mass relative to the starting point. This observation suggests that the process that leads to the peak c' is potential dependent and that it does not correspond to removal of a specific amount of Bpy in each experiment. The potential of the peak depends on several factors. For example, in Figure 23 a shift in the position of the peak c' is observed at the two different scan rates employed, but the thicknesses of the films were different because the experiments were carried out at two different scan rates within the same potential limits. When films of equal thickness (within 10%) were developed (by monitoring the mass increase) at -1.25V and the potential was scanned back to 0.0V at two different scan rates the increase in current that led to the peak c' occured at -0.8V (10 mV/s) and at -0.73V (50 mV/s). The complete removal of the film was accomplished at -0.57V for the slower scan (10mV/s) but was not complete for the faster scan (50 mV/s) even when the potential was at 0.0V. This could be judged from the fact that the current and mass response

returned to their starting values in the case of the scan at 10 mV/s but this was not the case at 50 mV/s. Thus, in spite of the large re-oxidation current leading to the peak c', re-oxidation of reduced Bpy is still quite slow.

4.7 The effect of the potential profile on the re-oxidation behaviour.

In the previous section we have seen under the conditions of the experiment at 10 mV/s in Figure 23 it was possible to achieve complete removal of film, but at a scan rate of 50 mV/s film removal was still not complete at 0.0V. Interestingly, further experiments showed that films of reduced Bpy could be completely removed even at quite low potentials if sufficient time is provided for the re-oxidation. Thus the potential was scanned to -1.3V and was held for a certain time until a film of desired thickness was formed (monitored by the increase in mass) and the potential was then scanned back to -0.9V and held for several minutes until the mass decreased to its starting value (this behaviour is schematically represented by a vertical arrow in Figure 23). During the holding time at -0.9V there was also a decrease in the oxidation current, while scanning the potential back to 0.0V showed no peaks. The current response also returned to the same level prior to the growth of film. The mass response from -0.9 V to 0.0V was also

completely flat. This indicates that complete film removal was achieved in this experiment. Clearly when thicker films are formed, the removal of films starts when the reduced Bpy begins to oxidize (at about -0.9V) but unless the scan is very slow, the films are not completely removed, even after the observation of peak c'.

Further experiments were carried out to investigate the re-oxidation process in more detail. The resulting cyclic voltammogram and mass response is shown in Figure 24. Here the potential was scanned to -1.2V at 50 mV/s and the film thus formed was monitored through the mass response. Then the potential was scanned to -0.9V at 50 mV/s and held for a time which was not sufficient for complete film removal. The potential scan was then continued to 0.0V and both the current and mass were recorded. This procedure introduces an additional peak (d') at -0.73V into the voltammetry and the usual peak c', which had a noisy structure, at -0.45V. If films of same thickness were grown and then during the scan if the potential was held at -0.9V for a shorter time, the peak d' was found to diminish and peak c' increased, whereas when the holding time was increased the reverse seems to be true. This suggests that a rough correlation exists between the peak c' and the amount of mass remaining on the electrode surface and the size of the peak d' and the amount of material removed from the electrode. This

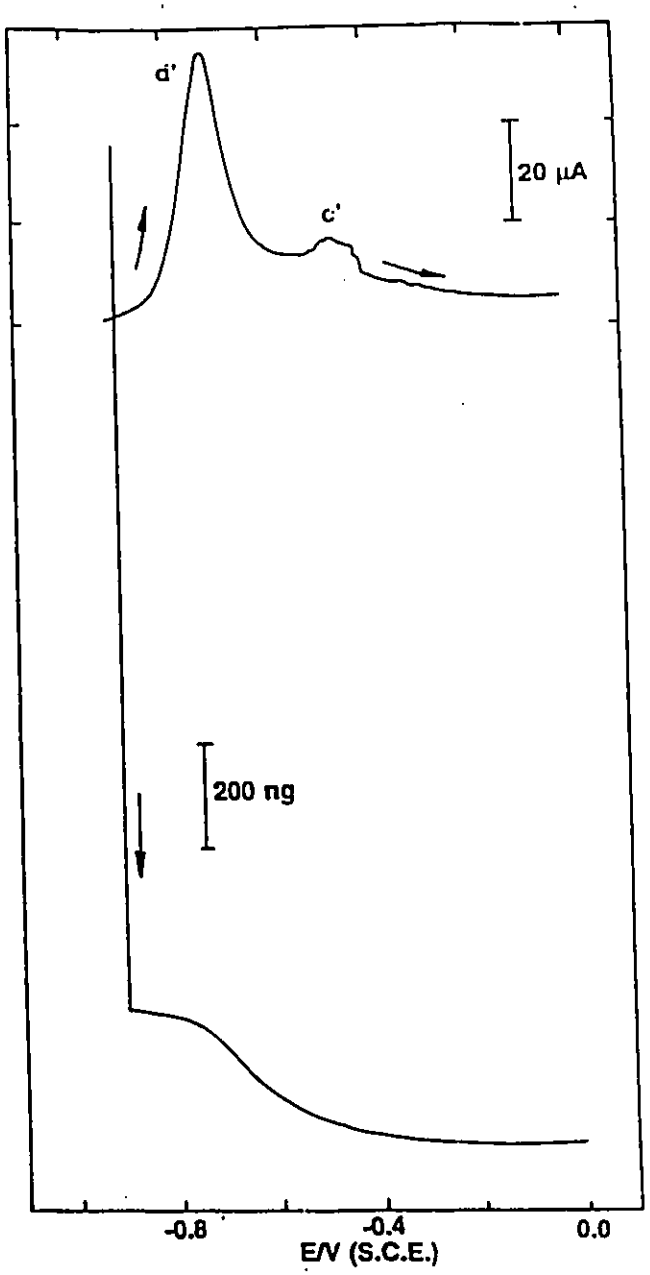

Figure 24. Cyclic voltammogram and mass response for removal of a film of reduced bipyridyl grown by pausing at -1.2V after a scan from 0.0V.

The potential was then scanned to -0.9V and held for a certain time before resuming the sweep in the positive going direction at 50mV/s. The mass response shows the decline in mass during holding while the current is illustrated from the point at which the scan was restarted. At the end of the scan the mass has returned to its starting value.

gives rise to two possibilities:-

1. First, when the potential is held at -0.9V for partial removal of the film the reduced Bpy is oxidized and may form the cation radical $BpyH^{+\cdot}$ in solution which may undergo further oxidation or diffuse into the bulk of the solution depending on the rates of the two competing processes. On restarting the scan, further oxidation of the cation radical could give the peak d' and the size of this peak would depend on the holding time and the amount of material removed from the electrode surface.

2. The second possibility is that when the potential is held at -0.9V some amount of material may be removed from the electrode and the remaining material may be redistributed between two states, one that is oxidized more easily forming the peak d' and the other that is oxidized in the usual peak c'.

It is difficult to know which option is correct, but the mass response indicates that there is some mass loss on the onset of peak d', which suggests it does not correspond to re-oxidation of cation radicals in solution, since we would not expect a mass change for oxidation of a solution species.

Clearly the re-oxidation process is complex and depends a little on film thickness. Thin films do not show the peak c' while thick films do, although even for thick films complete removal of reduced Bpy films can be achieved if sufficient time is allowed with the potential held at quite negative

potentials (-0.9V). Some aspects of this behaviour are discussed further below.

4.8 Conclusions.

In this chapter we have seen that when 4,4'bipyridyl is reduced at silver electrodes films of reduced Bpy are formed at the electrode surface. The films can be grown on the electrode either by cyclic voltammetry or a potential step experiment, provided the potential is taken to a sufficiently negative value. It is seen that if the potential is taken too negative (into the hydrogen evolution region), the formation of film ceases for some time and some material is actually lost from the electrode surface but if reduction of Bpy is re-activated by a small increase in potential then the growth of the film starts again. An approximate estimation shows that about 12 monolayers of reduced Bpy are formed on the electrode without any significant decrease in the rate of film growth. This type of film formation is verified by SERS studies on an Ag electrode which have shown that if the potential is held at an appropriately negative value, doubly reduced species of the form $BpyH_2$ are formed on the electrode surface[50].

The process of re-oxidation of reduced Bpy films is quite complex. At

the end of a cycle the film formed is not completely removed in the case of a scan at 50 mV/s to -1.3V (Figure 20, curve 2) except for thin films unless sufficient time is provided. Complete film removal can be achieved at quite negative potentials (-0.9V) as long as sufficient time is allowed. An unusual behaviour is exhibited by thicker films, there is some oxidation at lower potentials and the mass decreases since some material is removed from the electrode surface and then a second removal process is observed that leads to the unusual noisy peak c' which is accompanied by a change in the slope of the mass decrease. When films of equal thickness are removed at different scan rates, peak c' shifts to higher potentials at faster scan rates indicating a kinetic barrier to this process. This peak does not correspond to the removal of the last or several monolayers of material from the electrode surface, but to a process which is potential dependent and the position of this peak depends strongly on the amount of material remaining on the electrode surface. The EQCM can thus be used to study the growth and removal of the reduced Bpy films by providing a means to correlate the current response upon film removal with the amount of material on the electrode surface.

The nature of the oxidation process has not been clearly established. The peak c' which appears in the reverse scan was associated with the generation of a cation radical at the electrode as deduced from the SERS

studies from the observation of a purple coloured radical in solution[50]. This suggests that in this case the re-oxidation process may take place in two consecutive steps rather than one two-electron process. Some insight into the mechanism can be gained from the electrochemistry of the viologens which are similar to 4,4'bipyridyl but which have an alkyl group attached to the nitrogen. Thus methyl viologen is 4,4' bipyridyl with two methyl groups attached, one to each nitrogen. The cation radical formed from Bpy has (taking the reported behaviour of viologens as a guide) several possible fates[68] ; diffusion into bulk of solution, re-oxidation by traces of molecular oxygen, dimerization, disproportionation, formation of charge transfer complexes with the doubly reduced form of Bpy and also precipitation as a radical cation salt[62].

The shape of the peak c' varied considerably, it had a noisy structure or appeared as a wave in some cases, but in some experiments at slow scan rates very sharp peaks were observed that could be due to the oxidation of a film that exists in different energetic states. In the literature it has been reported that viologen radical films could recrystallise in a few seconds and produce areas of deposited film that are not available for direct oxidation. This behaviour depends strongly on different experimental conditions[71]. In the case of a heptyl cation radical film it has been reported that when the

potential is held in the cathodic region for a short time significant changes in the subsequent anodic current behaviour was found. This gives a clear indication that the behaviour of cation radical films is highly complex and this may also be the case of the doubly reduced bipyridyl films reported here. It is not possible to be more specific than this without further experiments.

REFERENCES

1. H. Abruna, In situ studies of electrochemical interfaces, VCH Chemicals, New York, 1991.
2. J. H. Kaufman, K. K. Kanazawa, G. B. Street, Phys. Rev. Lett., (53), 2461, 1984.
3. S. Bruckenstein, S. Swathirajan, Electrochim. Acta, (30), 851, 1985.
4. S. Bruckenstein, M. Shay, Electrochim. Acta, (30), 1295, 1985.
5. S. Bruckenstein, M. Shay, J. Electroanal. Chem. Interfacial. Electrochem. (188), 138, 1985.
6. M. R. Deakin, T. T. Li, O. R. Melroy, J. Electroanal. Chem., (243), 343, 1988.
7. C. Lu, A. W. Czanderna, "Applications of Piezoelectric Quartz Crystal Microbalance", Elsevier, 1984.
8. J. F. Alder, J. J. McCallum, Analyst, (108), 1291, 1983.
9. W. H. King, Jr., U. S. Patent, 3 164 004, 1965.
10. W. H. King, Jr., Res. Dev., 20 (4), 28, 1969.
11. W. H. King, Jr., Res. Dev., 20 (5), 28, 1969.
12. W. H. King, Jr., Anal. Chem., (36), 1735, 1964.
13. D. A. Buttry, M. D. Ward, Chem. Rev., (92), 1355, 1992.

14. H. E. Hager, R. D. Ruedisueli, M. E. Buehler, Corrosion, (42), 345, 1986.

15. W. D. Hinsberg, C. G. Willson, K. Kanazawa, J. Electrochem. Soc. (133), 1448, 1986.

16. C. Gabrielli, M. Keddam, H. Takenouti, Corrosion Science, (31), 129, 1990.

17. G. G. Guilbault, Anal. Chem.. (55), 1682, 1983.

18. M. Thompson, C. L. Arthur, K. D. Gurbaksh, Anal. Chem., (58), 1206, 1986.

19. F. W. Maarsen, M. C. Smit, J. Martz, Rev. Trav. Chim. Pays-Bas, (76), 713, 1957.

20. F. C. Phillips, "An Introduction to Crystallography", Third Edition, Longmans, London, 155, 1963; Fourth Edition, Oliver and Boyd, Edinburgh, 167, 1971.

21. G. Lippmann, An. Chim. Phys., Ser.5, (24), 145, 1881.

22. D. A. Buttry, "Electroanalytical Chemistry", (A. J. Bard, ed.), Marcel Dekker, New York, Vol.17, 1, 1991.

23. R. A. Heising, "Quartz Crystal for Electrical Circuits", Van Nostrand, New York, N. Y., 24, 1946.

24. J. Hlavay, G. G. Guilbault, Anal. Chem., (49), 1890, 1977.

25. G. Z. Sauerbrey, Phys. Verhandl, (8), 113, 1957.

26. G. Z. Sauerbrey, Z. Phys., (115), 206, 1959.

27. C. S. Lu, O. Lewis, J. Appl. Phys., (43), 4385, 1972.

28. P. L. Konash, G. J. Bastiaans, Anal. Chim., (52), 1929, 1980.

29. T. Nomura, Anal. Chim. Acta, (124), 81, 1981.

30. Yao ShouZhou, ZhouTiean, Human Daxue Xuebao, (15), 1988, 1.

31. K. K. Kanazawa, J. G. Gordon, Anal. Chim. Acta, (175), 99, 1985.

32. K. K. Kanazawa, J. G. Gordon, Anal. Chem., (57), 1770, 1985.

33. M. Thompson, A. L. Kipling, W. C. Duncan-Hewitt, L. V. Rajakovic and B. A. Cavic-Vlasak, Analyst, (116), 881, 1991.

34. K. R. Grebe, J. V. Powers, Brit. Patent 1047789, 9 November, 1966.

35. M. F. L. de Mele, R. C. Salvarezza, V. D. Vasquez Moll, H. A. Videla, A. J. Arvia, J. Electrochem. Soc., (133), 746, 1986.

36. K. Sakamaki, K. Itoh, A. Fujishima, Y. Goshi, J. Vac. Sci. Technol A (8), 530, (1990).

37. I. Otsuka, T. Iwasaki, J. Vac. Sci. Technol A (8), 530, (1990).

38. M. L. Hitchman, F. W. M. Nyasulu, A. Aziz, D. D. K. Chingakule, Anal. Chim. Acta., (155), 219, 1983.

39. M. L. Hitchman, Anal. Chim. Acta., (171), 131, 1985.

40. M. L. Hitchman, A. Aziz, D. D. K. Chingakule, F. W. M. Nyasulu,

Anal. Chim. Acta., (171), 141, 1985.

41. Kh. Z. Brainina, Talanta, (18), 513, 1971.

42. J. Wang in "Stripping Analysis, Principles, Instrumentation and Applications" 1985, VCH publishers, Deerfield Beach, Florida.

43. M. Hepel, R. A. Osteryoung, J. Electroanal. Chem., (149), 193, 1983.

44. M. Iwamoto, R. A. Osteryoung, J. Electroanal. Chem., (169), 181, 1984.

45. E. S. Grabbe, R. P. Buck, O. R. Melroy, J. Electroanal. Chem., (223), 67, 1987.

46. Y. C. Wu, P. Zhang, H. W. Pickering, D. L. Allara, J. Electrochem. Soc., (140) 2791, 1993.

47. S. F. L. Da. Costa, S. M. L. Agostinho, K. Nobe, J. Electrochem. Soc., (140), 3483, 1993.

48. T. M. Cotton, D. Kaddi, D. Iorga, J. Amer. Chem. Soc., (105), 7462, 1983.

49. T. M. Cotton, M. Vavra, Chem. Phys. Lett., (106), 491, 1984.

50. T. Lu, T. M. Cotton, R. L. Birke, J. R. Lombardi, Langmuir, (5), 406, 1989.

51. CRC Handbook of Chemistry and Physics, ed. D. R. Lide 73rd edition 1992-3 CRC Press.

52. R. Schumacher, G. Borges, K. K. Kanazawa, Surf. Sci., (163), L621, 1985.

53. R. Schumacher, J. G. Gordon, O. R. Melroy, J. Electroanal. Chem., (216), 127, 1987.

54. K. Itaya, S. Sugawara, K. Sashikata, N. Furuya, J. Vac. Sci. Technol A (8), 515, 1990.

55. K. Sashikata, N. Furuya, K. Itaya, J. Vac. Sci. Technol B (9), 457, 1991.

56. W. J. Peard, R. T. Pflaum, J. Amer. Chem. Soc., (80), 1593, 1958.

57. T. R. Musgrave, C. E. Mattson, Inorg. Chem., (7), 1433, 1968.

58. I. S. Ahuja, R. Singh, C. P. Rai, J. Inorg. Nucl. Chem., (40), 924, 1978.

59. M. Donten, J. Osteryoung, J. Electrochem. Soc., (138), 82, 1991.

60. J. Volke, V. Volková, Collect. Czech. Chem. Commun., (37), 3686, 1972.

61. M. Heyrovský, J. Chem. Soc. Faraday Trans. I, (82), 585, 1986.

62. M. Heyrovský, L. Novotný, Collect. Czech. Chem. Commun., (52), 54, 1987.

63. M. Heyrovský, L. Pospīsil, J. Electroanal. Chem., (225), 291, 1988.

64. K. Uosaki, H. A. O. Hill, J. Electroanal. Chem., (122), 321, 1981.

65. I. Taniguchi, M. Iseki, H. Yamaguchi, K. Yasukouchi, J. Electroanal. Chem., (186), 299, 1985.

66. C. P. Wilde, T. Ding, J. Electroanal. Chem., (327), 279, 1992.

67. M. J. Eddowes, H. A. O. Hill, J. Chem. Soc. Chem. Commun., (21), 771, 1977.

68. C. L. Bird, A. T. Kuhn, Chem. Soc. Rev., (10), 49, 1981.

69. M. Hepel, K. Kanige, S. Bruckenstein, J. Electroanal. Chem., (266) 409, 1989.

70. M. Hepel, S. Bruckenstein, K. Kanige, J. Chem. Soc., Faraday Trans., (89), 251, 1993.

71. J. Bruinink, C. G. A. Kregting, J. J. Ponjeé, J. Electrochem. Soc., (124), 1854, 1977.